Physics and Physical Oceanography Data Report 2013

Analysis of Physical Oceanographic Data from Lake Melville, Labrador, July - September 2012

Zhaoshi Lu, Brad deYoung, and Jack Foley

April 26, 2013

Department of Physics and Physical Oceanography
Memorial University of Newfoundland
St. Johns, Newfoundland
A1B 3X7

Abstract

A cruise was carried out during July 2012 in Lake Melville, a large and complex sub-Arctic fjord which serves as a major outlet for freshwater on the Labrador coast, to deploy oceanographic meters with which to collect data on the circulation and hydrography of Lake Melville. Two moorings were deployed to record current velocity, temperature, and salinity from July to September 2012. All the moorings included ADCP to measure water speed and thermistors to measure water temperature. One TDR-2050P Temperature and Depth Logger was deployed inside the Lake. Temperature, salinity and density profiles, were collected from CTD casts surveys made at 10 stations from September 7 to September 9. We present plots of the raw data, statistical analyses, and information on quality control processes.

Acknowledgements

We thank the captain and crew of the What's Happening for their help in the deployment and recovery of the instrumentation. We also acknowledge the support of NSERC and the NCE Arcticnet Program.

Contents

List of Figures

List of Tables

Chapter 1

Introduction

An estuary is a semi-enclosed coastal area of interaction between salt and fresh water. It has one or more rivers flowing into, and a free connection to the open sea. Fjord estuaries, formed by glacial erosion and generally occur at higher latitude. A fjord usually has a river/rivers running into the basin at its head, and a sill near its mouth to the open ocean, isolating the deeper waters of the fjord from the ocean. As a result, a fjords are often a highly stratified, with freshwater at the surface and trapped heavier sea water at the bottom. The typical fjord is relatively long and narrow and with a deep in the basin. The environment in fjord is generally the result of a dynamic balance between factors such as tides, river runoff and sea salinity, local meteorological conditions, and topography.

Hamilton Inlet is the largest inlet on the coast of Labrador and consists of Goose Bay, Lake Melville and Groswater Bay. Hamilton Inlet may be classified as a fjord-type estuary system, based on topography and degree of stratification. Hamilton Inlet serves as a major outlet for freshwater on the Labrador coast (Figure 1.1). Groswater Bay extends west for approximately 50 km, and it then constricts into a narrow shallow channel (known as the Narrows) of about 22 km in length, 2.5 km in width and 30 m in depth. Lake Melville extends west for 170 km from the Narrows, with a basin depth of over 200 m and a maximum width of 35 km. Goose Bay, a 22 km extension of Lake Melville, has a depth of over 60 m. Fresh water is discharged into the lake at the southwestern end by four major rivers (Churchill River, Northwest, the Kenamu, and the Goose, in order of size (Figure 1.2).

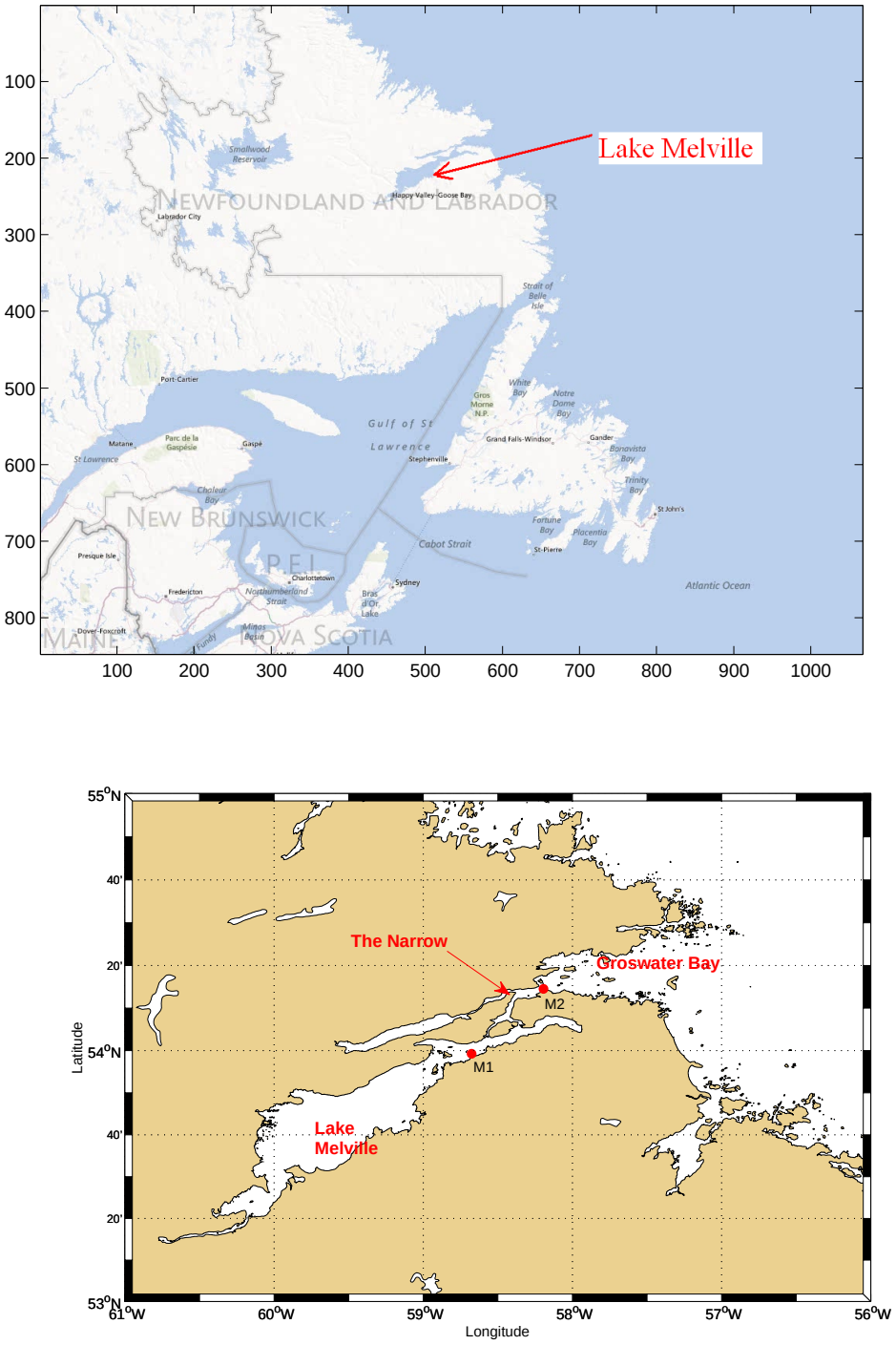

Figure 1.1: Location of Lake Melville, Labrador.

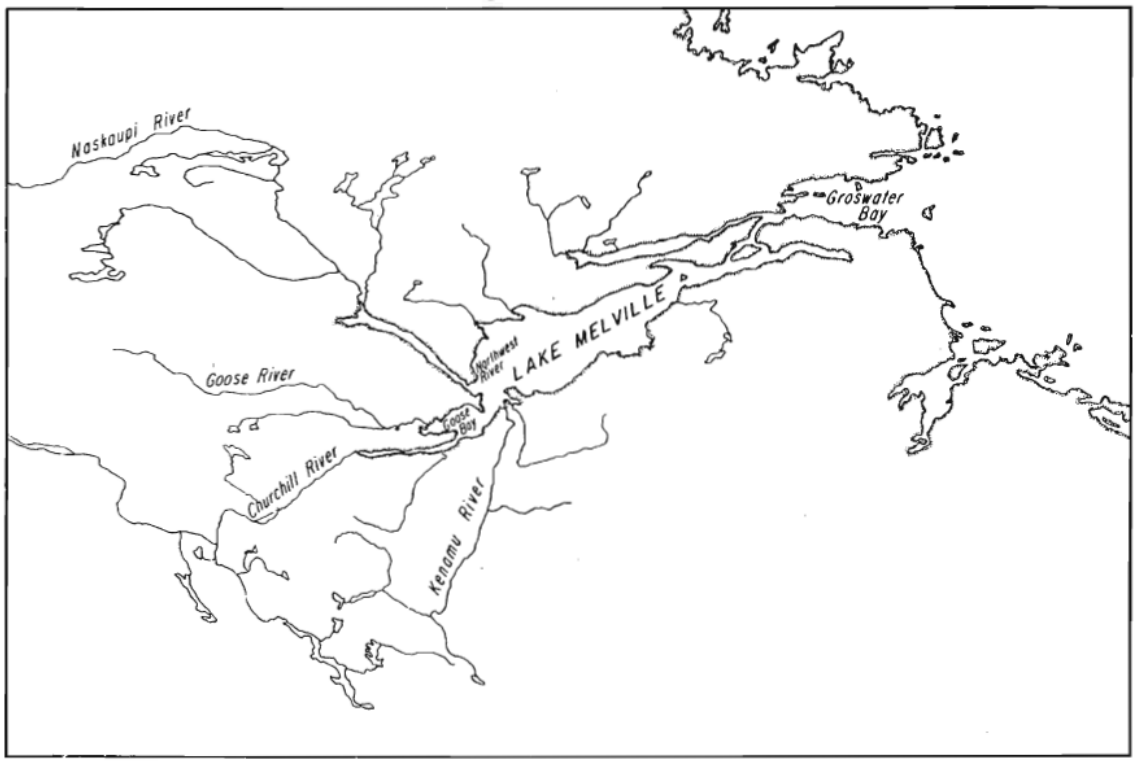

Figure 1.2: Major rivers flowing into Lake Melville.

Chapter 2

Measurements

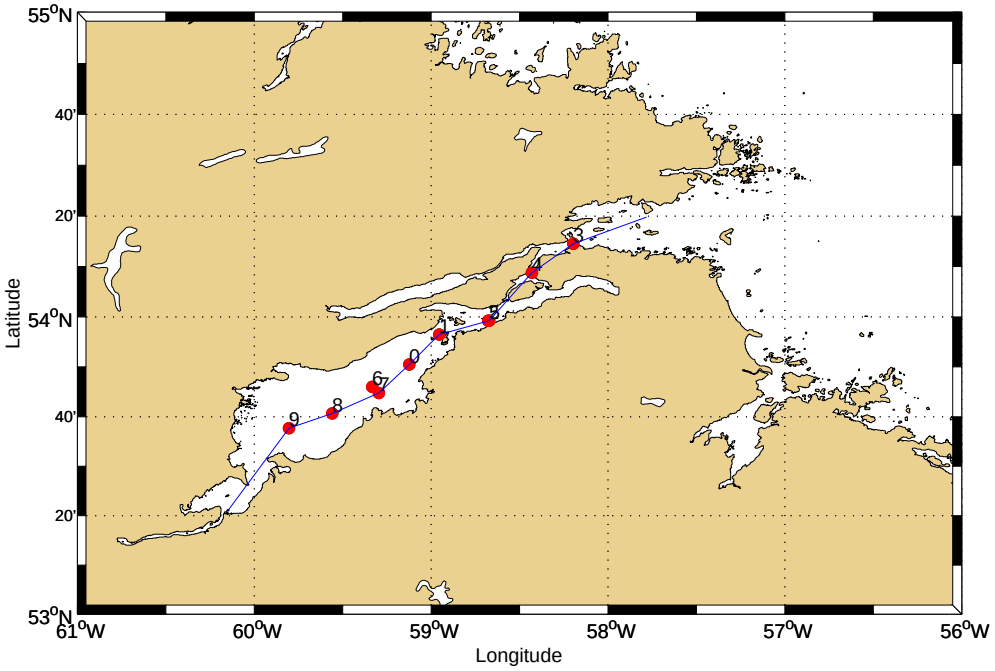

Figure 2.1: Hydrographic (CTD) casts surveys location, following the thalweg of the Lake Melville. Bottom figure shows the depth along the thalweg.

To investigate the exchange dynamics of the system near the Narrows of the Lake Melville, mooring measurements were performed at two stations. The locations of the instruments deployed are shown in Figure 1.1. Current data was collected with RDI Acoustic Doppler current profilers (ADCPs), at sites

M1 and M2. At mooring station M1, which is inside the lake, the water depth is 189 m. As the measurements range for RDI ADCP is about 106 m from the sensors, so two ADCPs were placed in the middle of the water column, with one ADCP moored at 95 meters above bottom looking upward and another moored at 97 meters above bottom looking downward. At mooring station M2 outside the lake, which is about 90 m in water depth, one RDI ADCP was moored about two meters above the bottom looking upward over the water column. All three ADCPs measured currents over the water column at 2 m spatial intervals and 20 minutes temporal intervals. Current measurements were taken from July 8th, 2012 to September 7th, 2012. The instruments were all RDI 4 beam Workhorse Broadband ADCPs working at 300 kHz frequency. All ADCPs were configured to collected data at the same 20 minutes temporal interval.

Water temperature data were collected with Vemco loggers thermistors mounted on each mooring. At station M1, thermistors was mounted at depths of 10, 15, 20, 25, 30, 35, 40, 50, 60, 70, 80, 90, 120, 140, 180 and 186 m. At station M2, thermistors was mounted at depths of 10, 15, 20, 25, 35,40, 60, 70, 80 and 100m. All thermistors collected data at the same 20 minutes temporal interval.

At station M1, a TDR-2050P Temperature and Depth Logger was deployed at a depth of about 7.7 m, attached to the buoy. Water temperature and absolute pressures were collected at an interval of 1 minute.

Hydrographic data, specifically temperature, salinity and density profiles, were collected from casts surveys made at about 10 stations from September 7 (day 250) to September 9 (day 252) (see Figure 2.1).

Table 2.1: Location and details of 2012 ADCP moorings.

Mooring	Latitude	Longitude	Depth (m)	Averaging Period	Bin Size
M1	53°59.234'N	058°40.527'W	192 m	20 Min	2 m
M2	54°14.539'N	058°11.645'W	106 m	20 min	2 m

A summary of mooring instruments and CTD casts is given in Tables 2.1 and 2.2.

Table 2.2: Location and details of 2012 CTD casts.

Cast #	Time	Latitude	Longitude	Depth (m)
0	9/07/2012 11:15	53°50.50'N	059°07.39'W	198
1	9/07/2012 13:27	53°56.44'N	058°57.15'W	55
2	9/07/2012 15:55	53°59.23'N	058°40.53'W	152
3	9/07/2012 19:34	54°14.54'N	058°11.65'W	105
4	9/08/2012 15:28	54°08.74'N	058°25.71'W	26
5	9/08/2012 19:18	53°59.22'N	058°40.30'W	171
6	9/08/2012 23:04	53°46.02'N	059°19.99'W	73
7	9/08/2012 23:25	53°44.75'N	059°17.59'W	202
8	9/09/2012 03:21	53°40.65'N	059°33.51'W	48
9	9/09/2012 04:44	53°37.70'N	059°48.21'W	76

Chapter 3

Plots of raw data

In this section, figures of raw instruments records are presented, including time series plots of selected ADCP depths, thermistors records, and TDR-2050P Temperature and Depth Logger records, and vertical profiles plots of CTD casts.

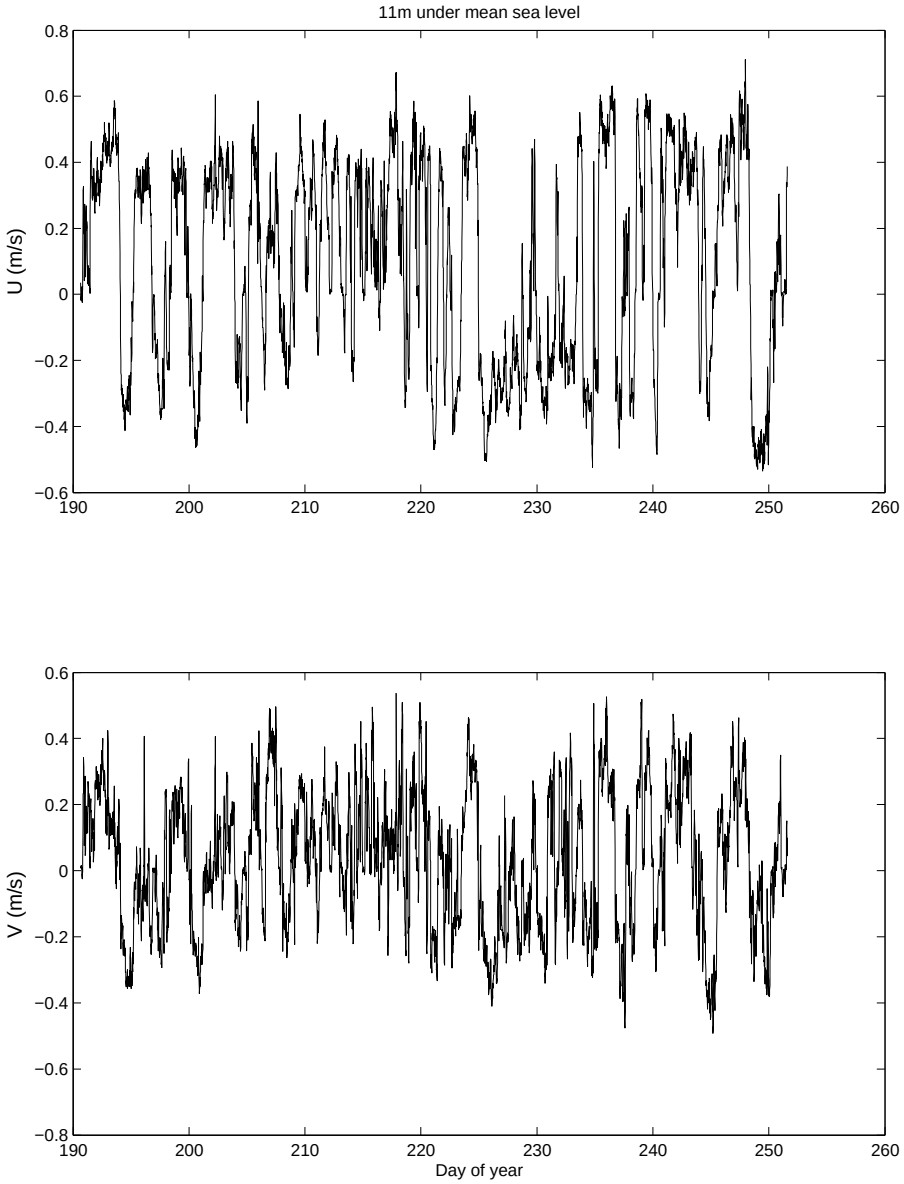

Figure 3.1: Time series plot of ADCP records at 11 m, M1.

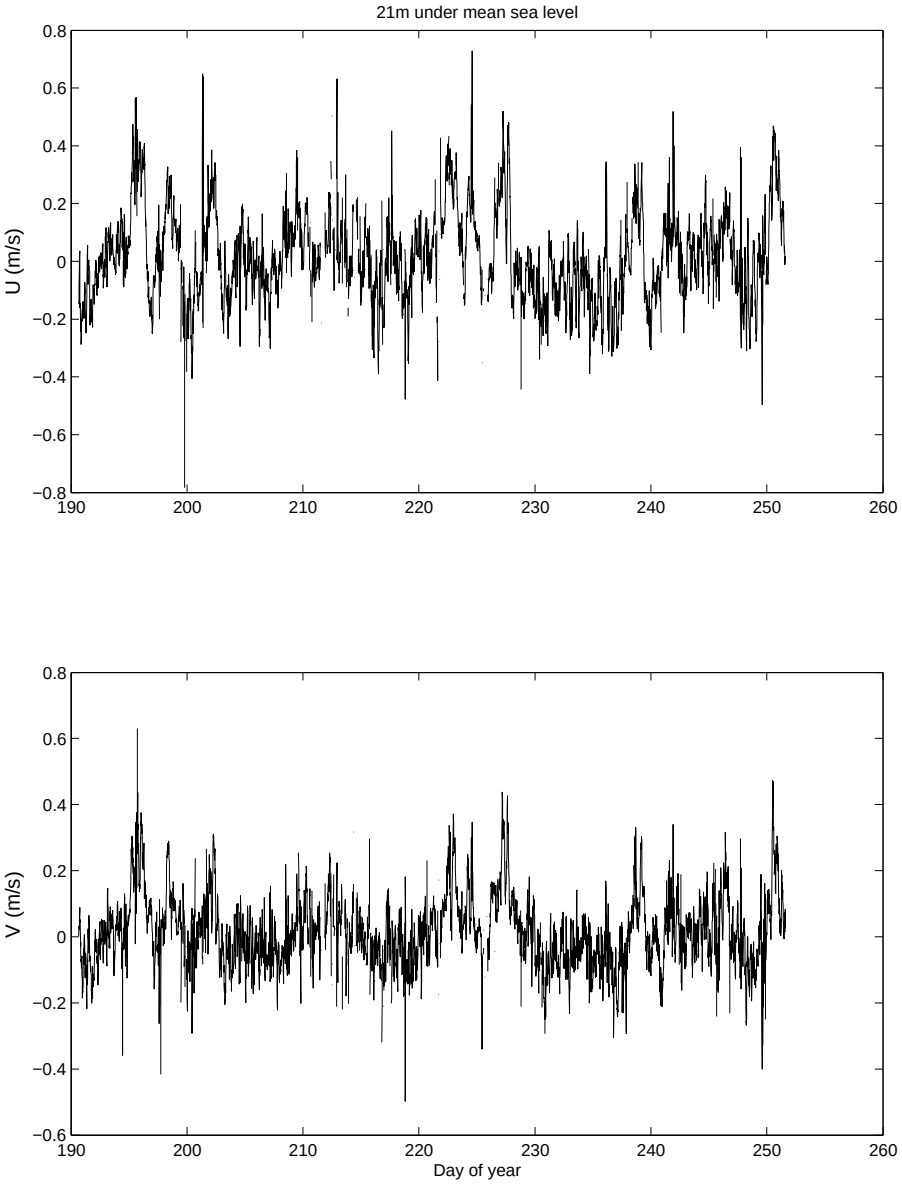

Figure 3.2: Time series plot of ADCP records at 21 m, M1.

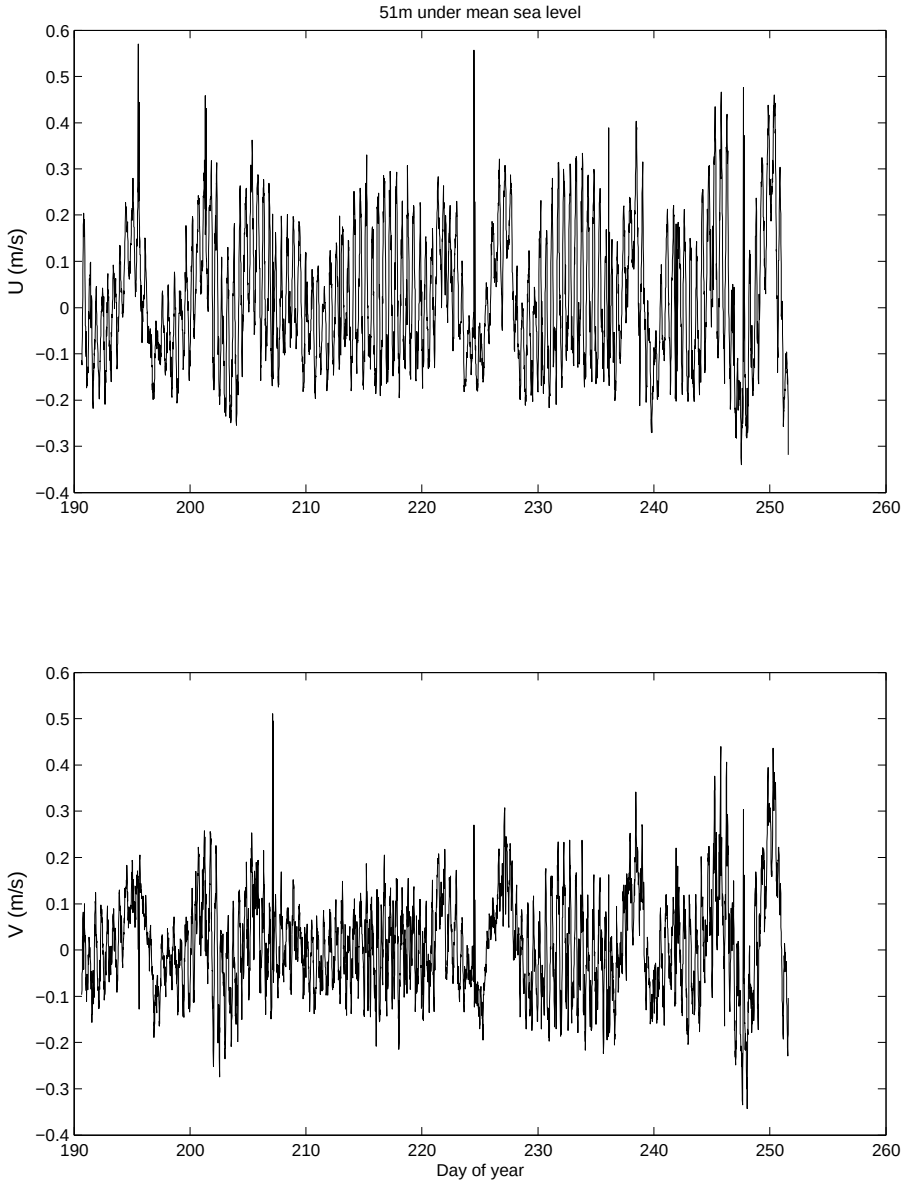

Figure 3.3: Time series plot of ADCP records at 51 m, M1.

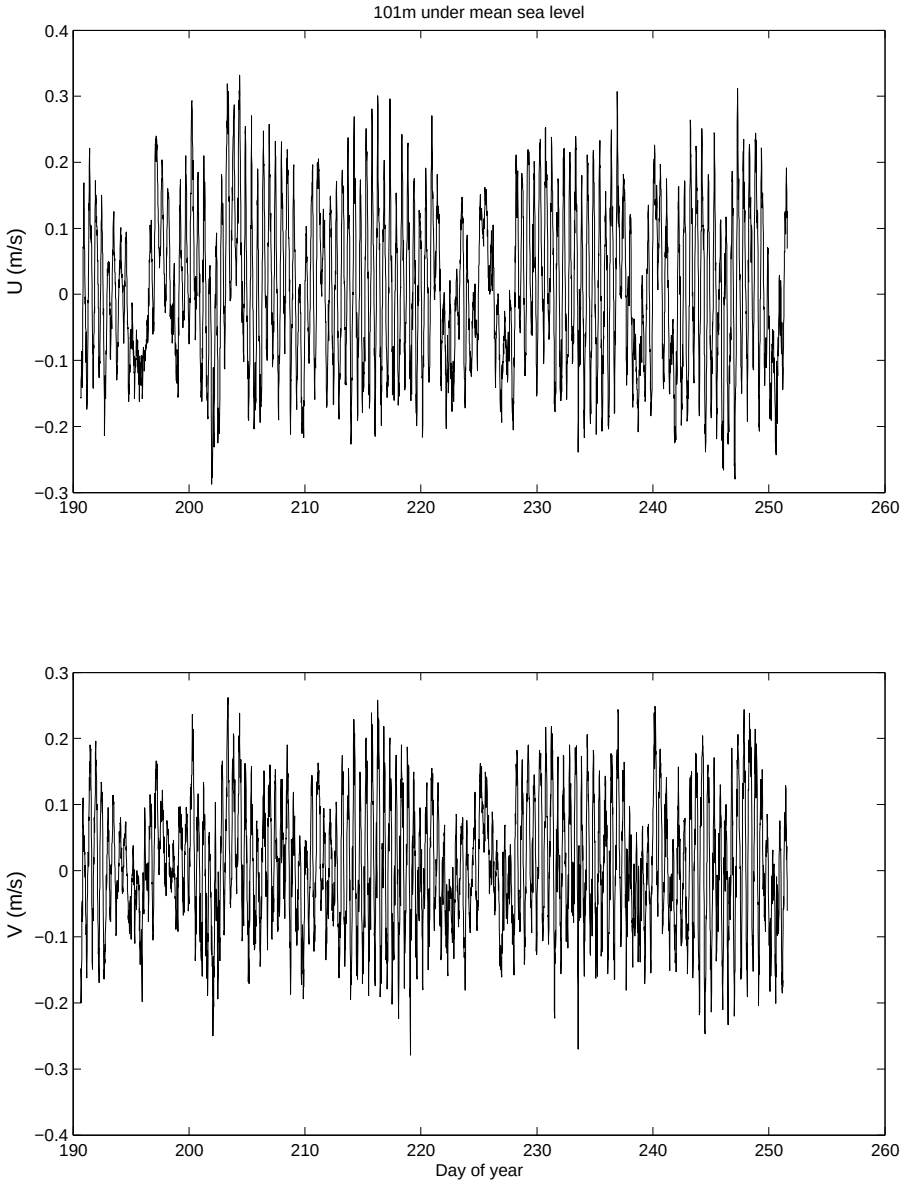

Figure 3.4: Time series plot of ADCP records at 101 m, M1.

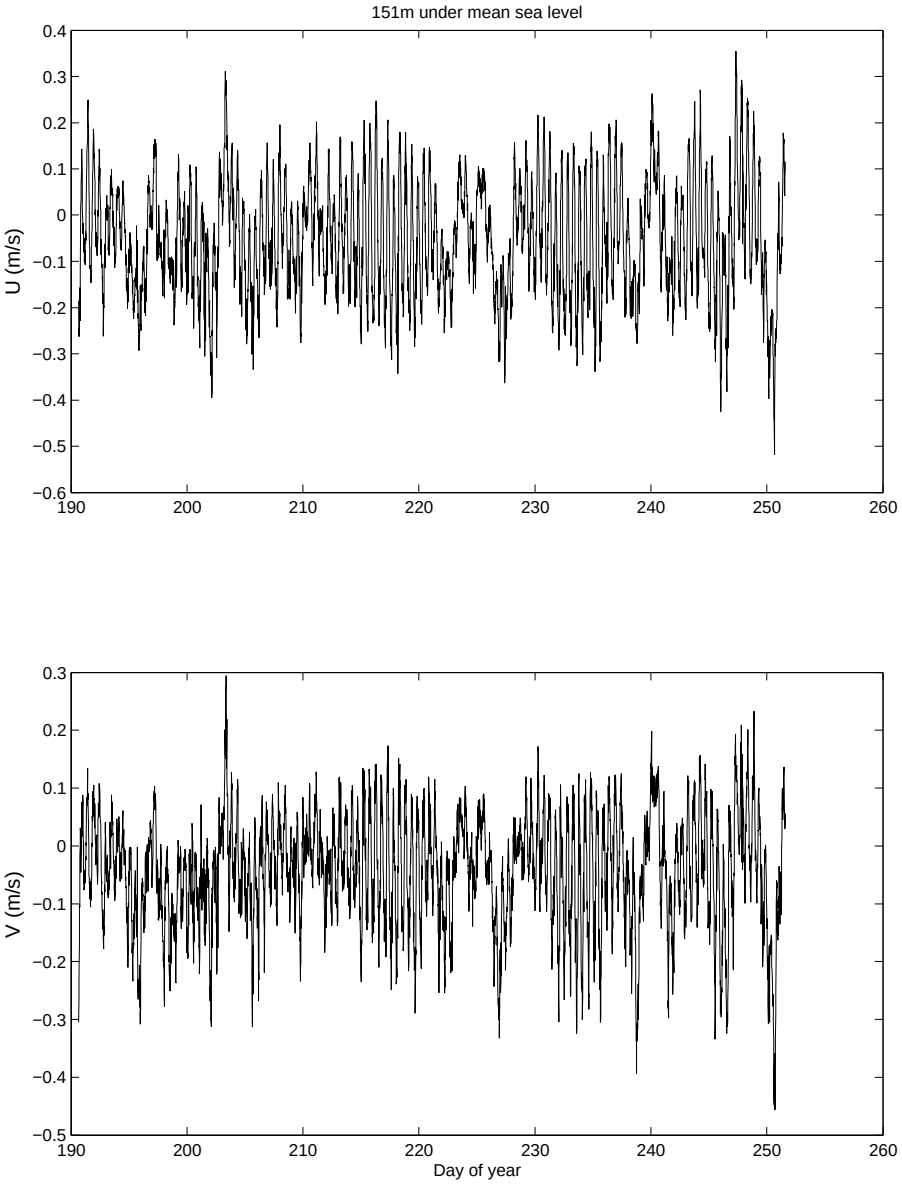

Figure 3.5: Time series plot of ADCP records at 151 m, M1.

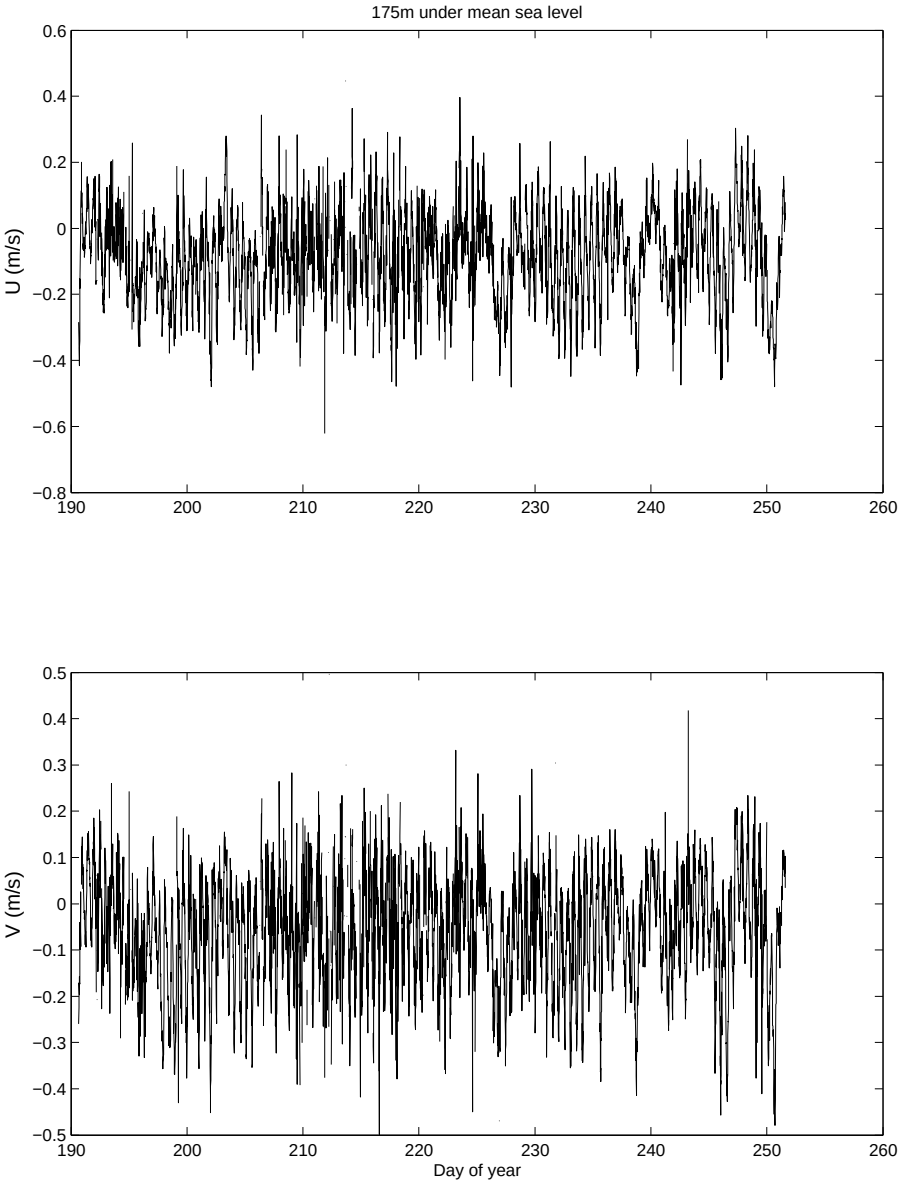

Figure 3.6: Time series plot of ADCP records at 175 m, M1.

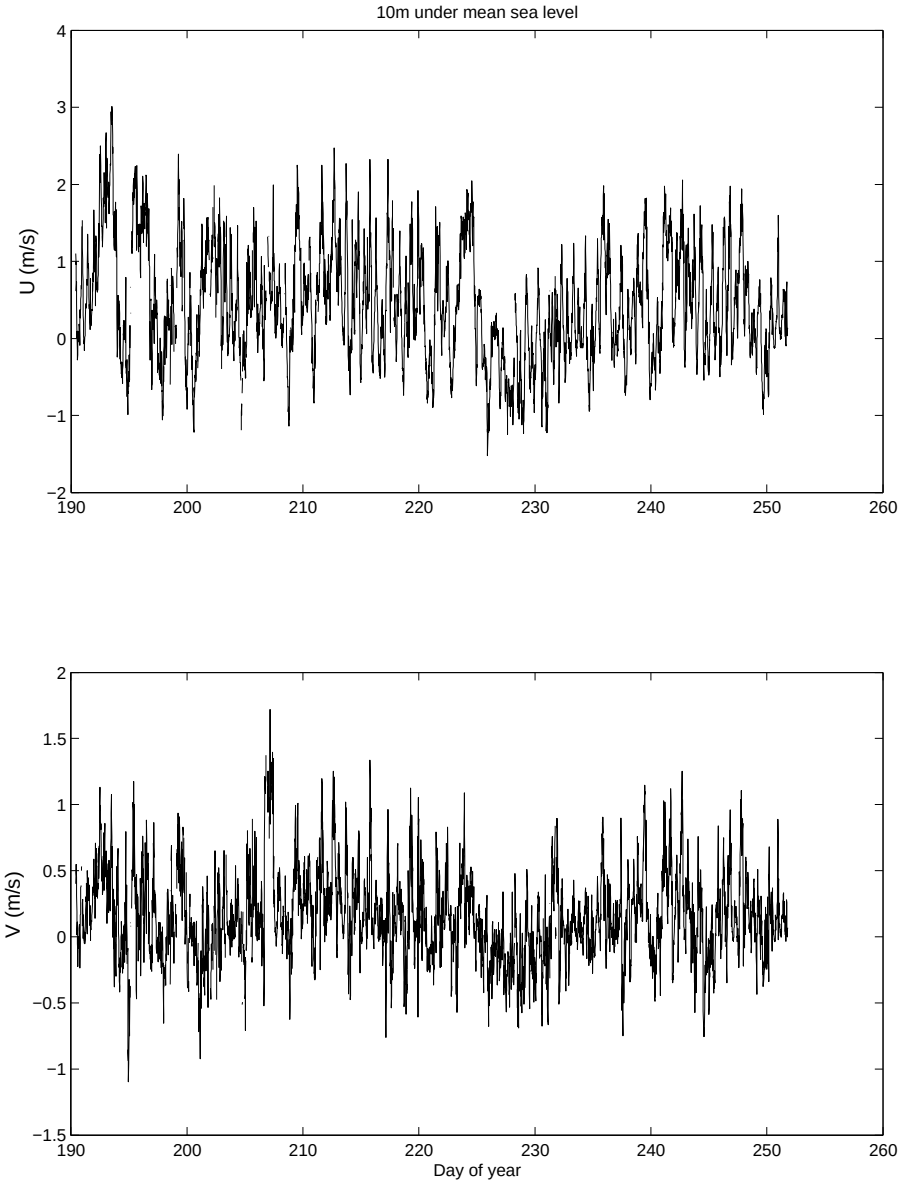

Figure 3.7: Time series plot of ADCP records at 10 m, M2.

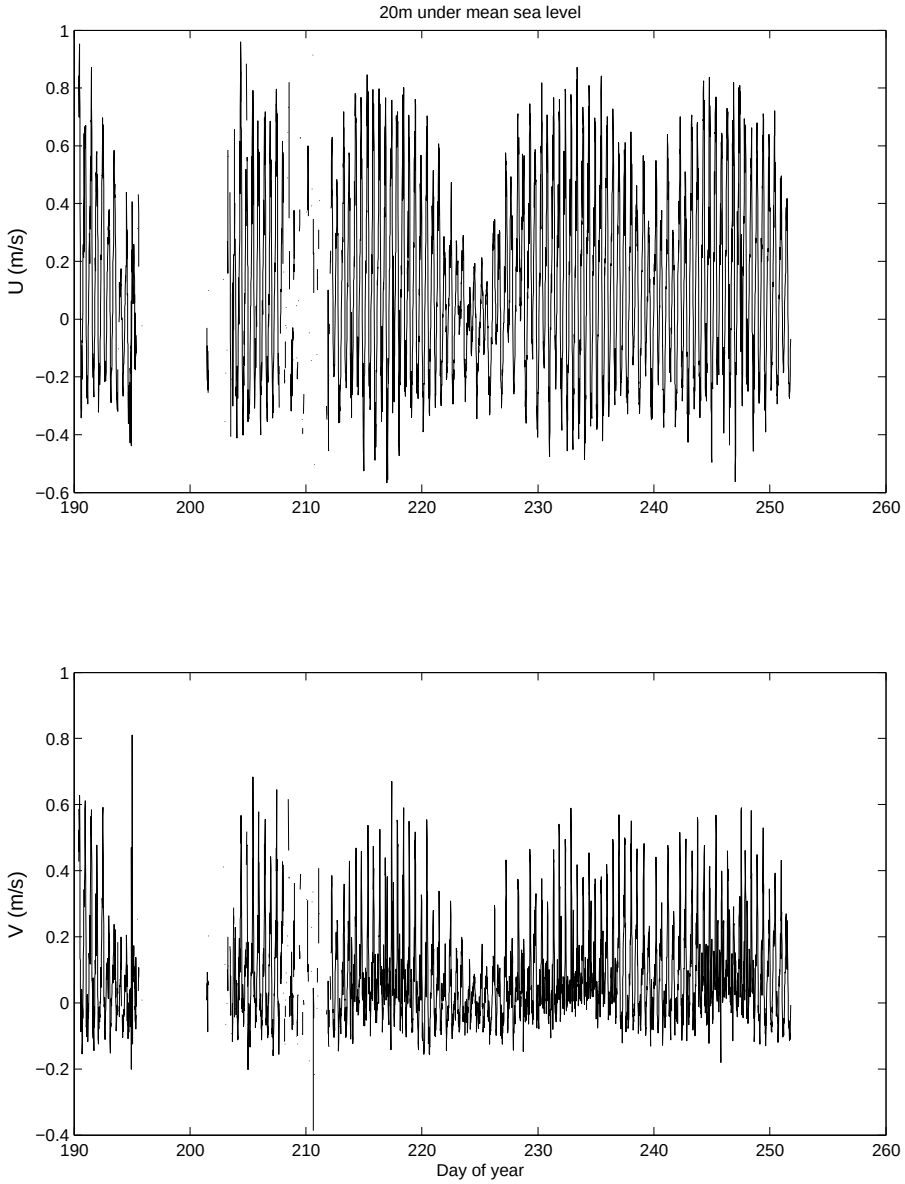

Figure 3.8: Time series plot of ADCP records at 20 m, M2.

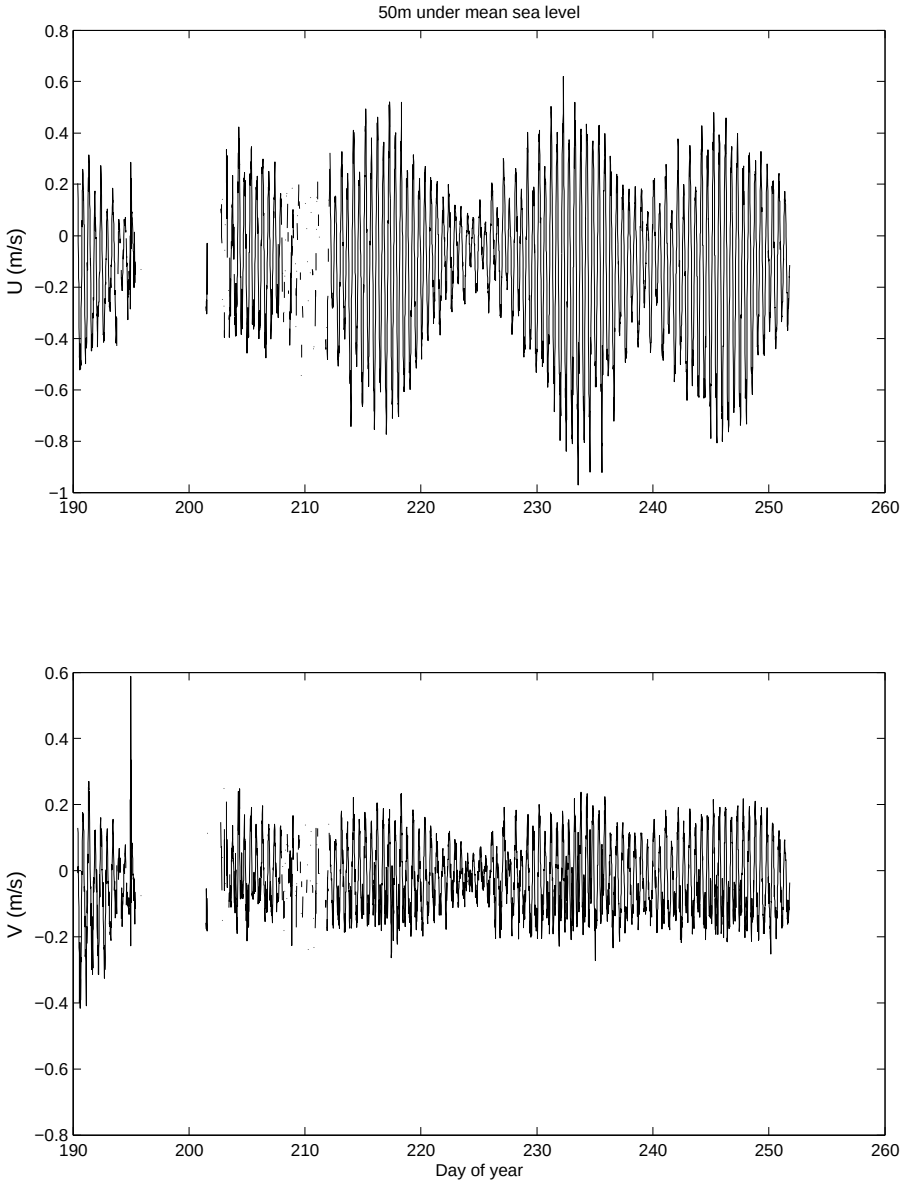

Figure 3.9: Time series plot of ADCP records at 50 m, M2.

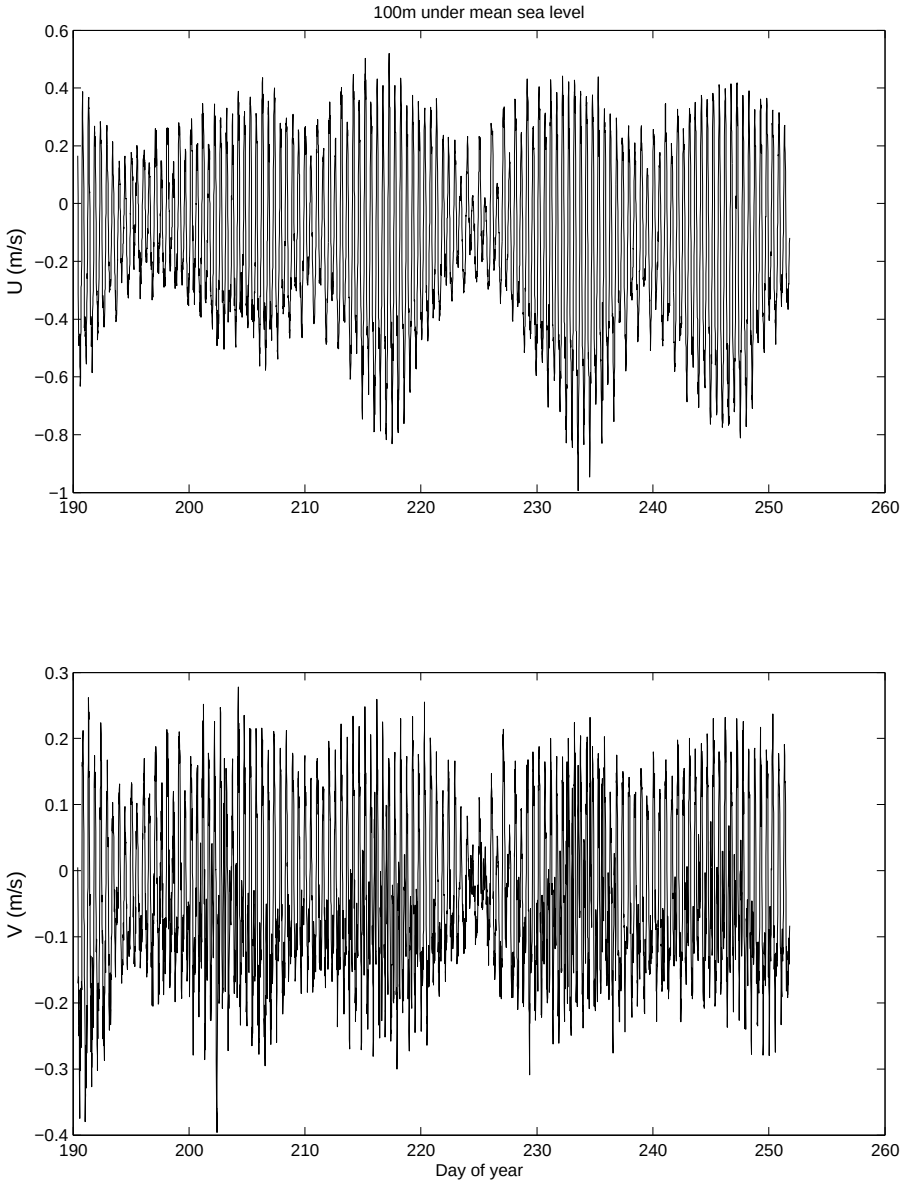

Figure 3.10: Time series plot of ADCP records at 100 m, M2.

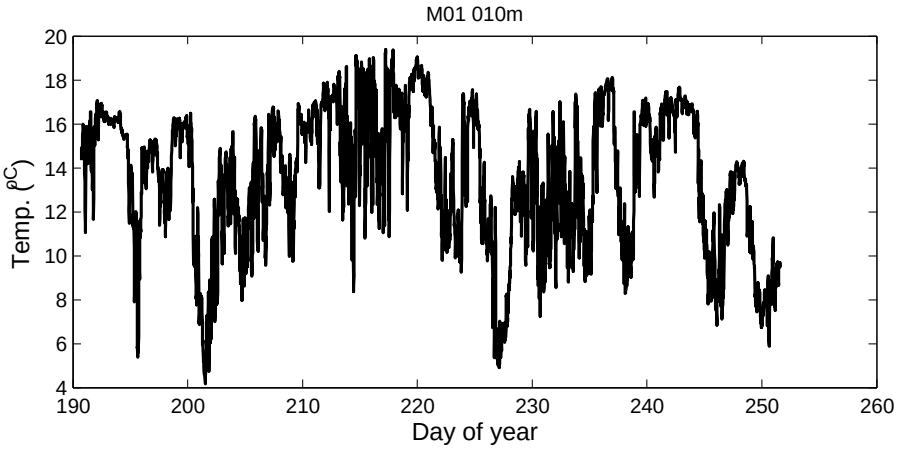

Figure 3.11: Time series plot of thermistors records at 10 m, M1.

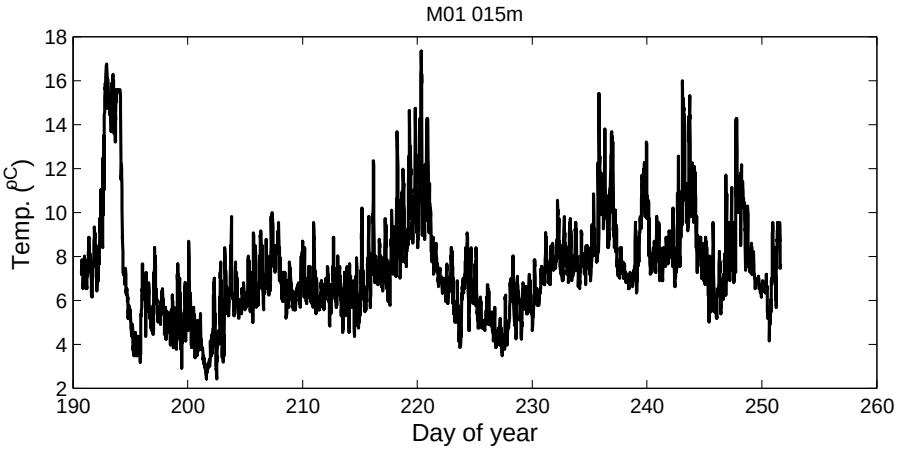

Figure 3.12: Time series plot of thermistors records at 15 m, M1.

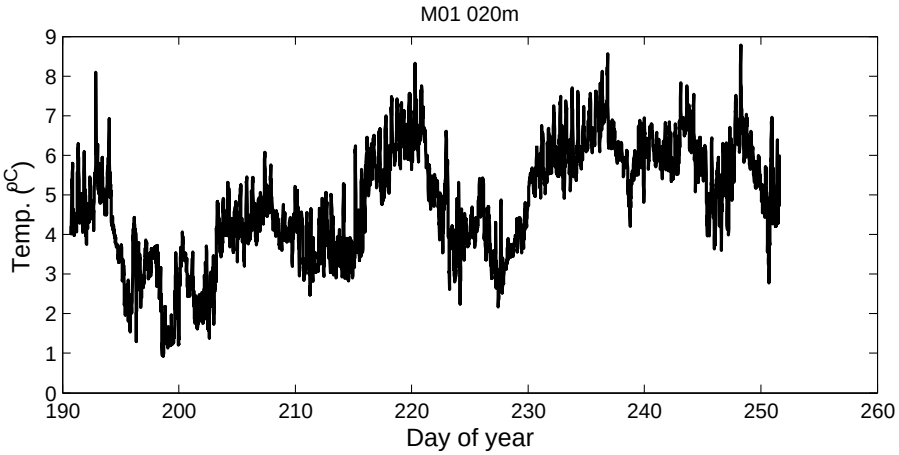

Figure 3.13: Time series plot of thermistors records at 20 m, M1.

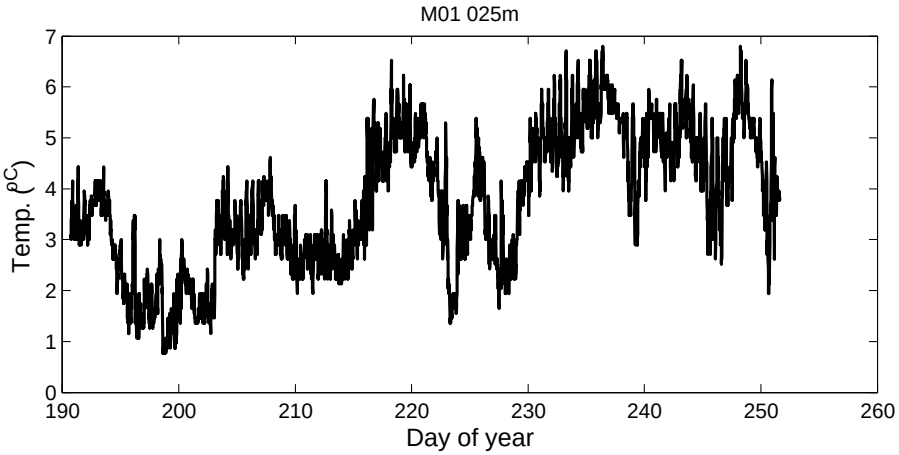

Figure 3.14: Time series plot of thermistors records at 25 m, M1.

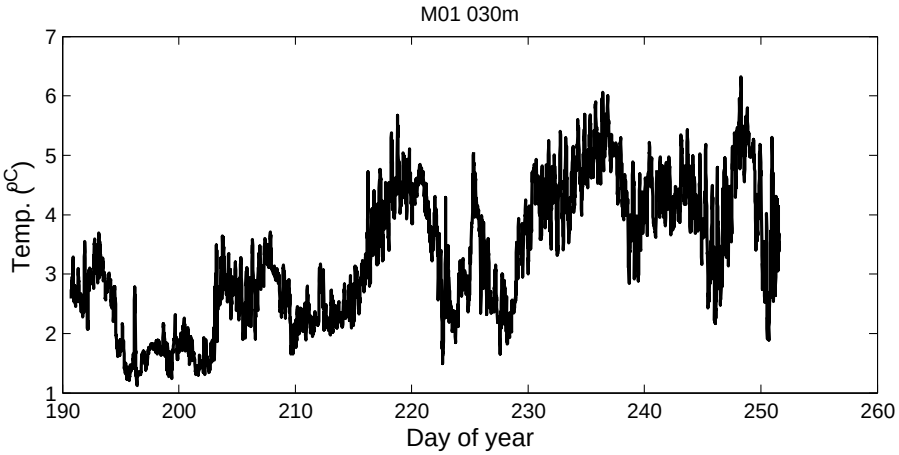

Figure 3.15: Time series plot of thermistors records at 30 m, M1.

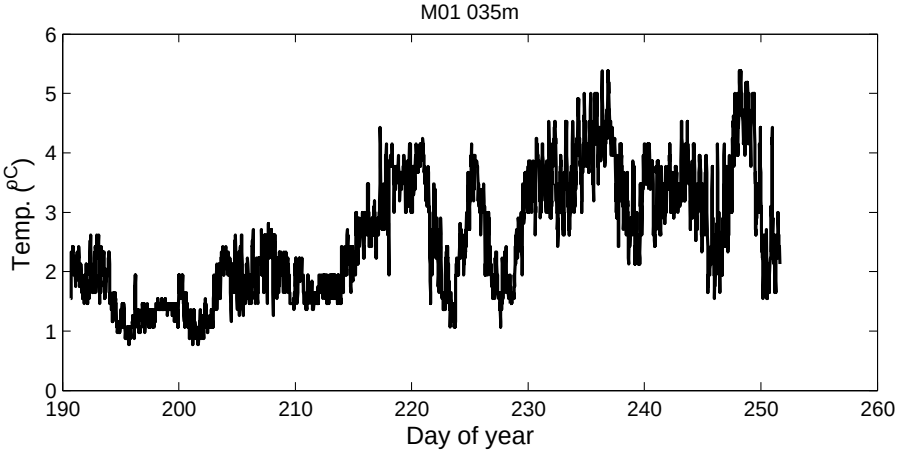

Figure 3.16: Time series plot of thermistors records at 35 m, M1.

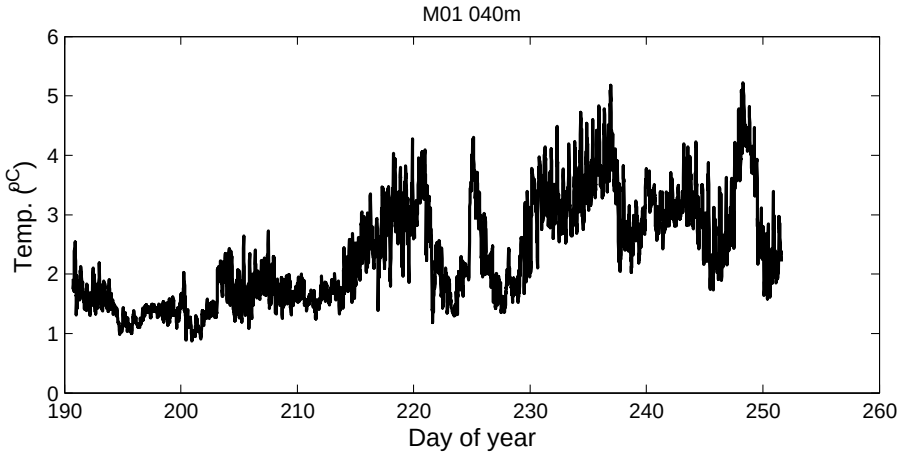

Figure 3.17: Time series plot of thermistors records at 40 m, M1.

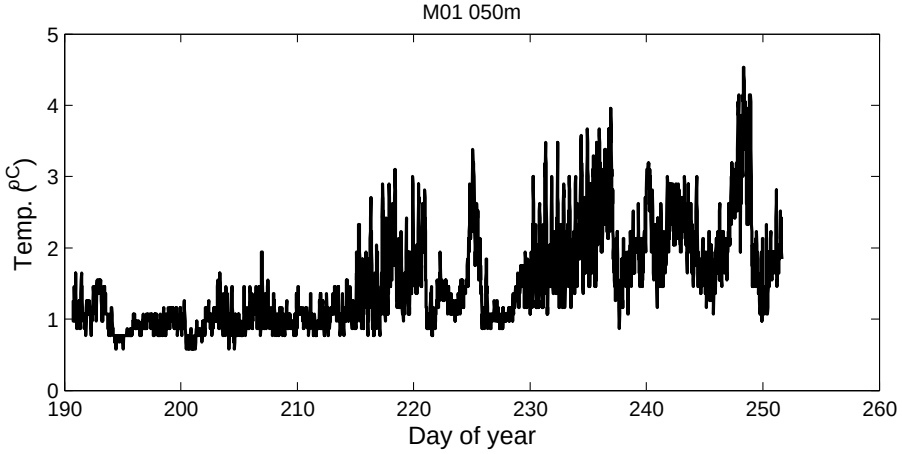

Figure 3.18: Time series plot of thermistors records at 50 m, M1.

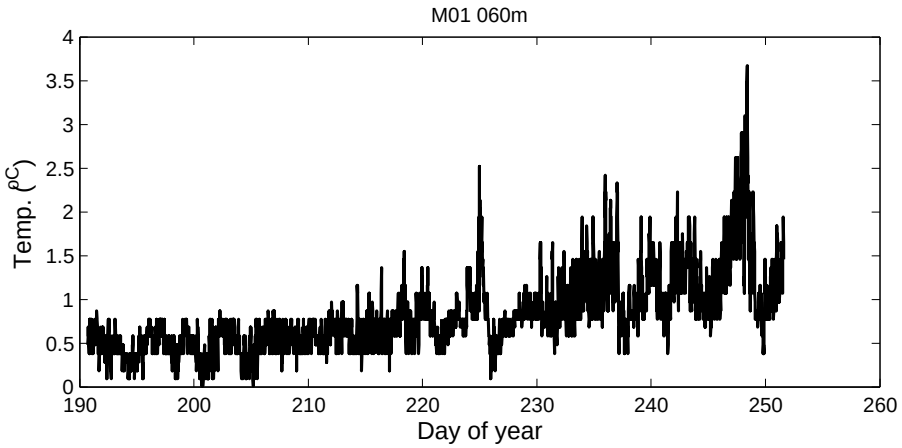

Figure 3.19: Time series plot of thermistors records at 60 m, M1.

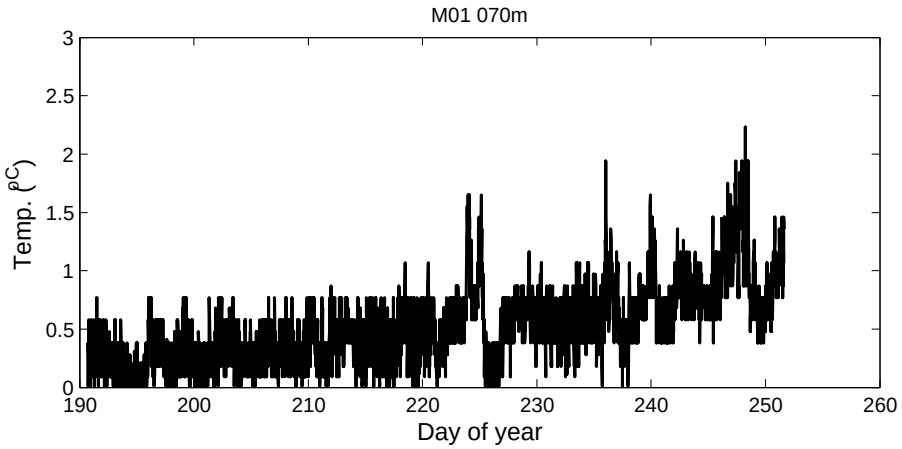

Figure 3.20: Time series plot of thermistors records at 70 m, M1.

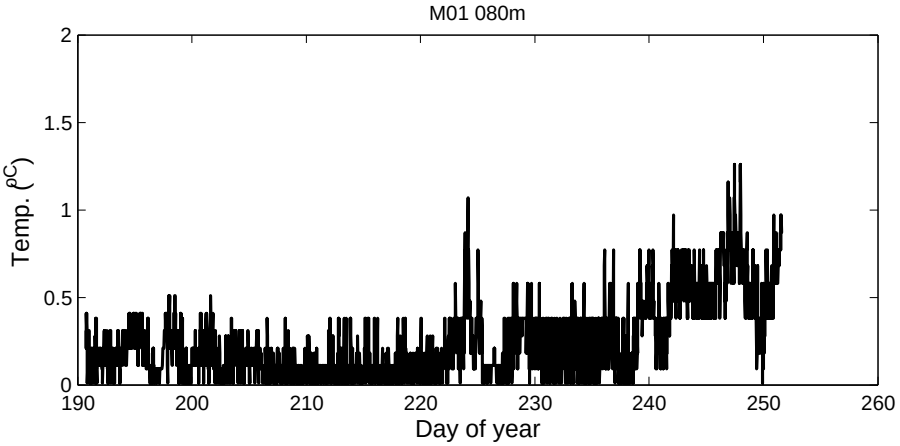

Figure 3.21: Time series plot of thermistors records at 80 m, M1.

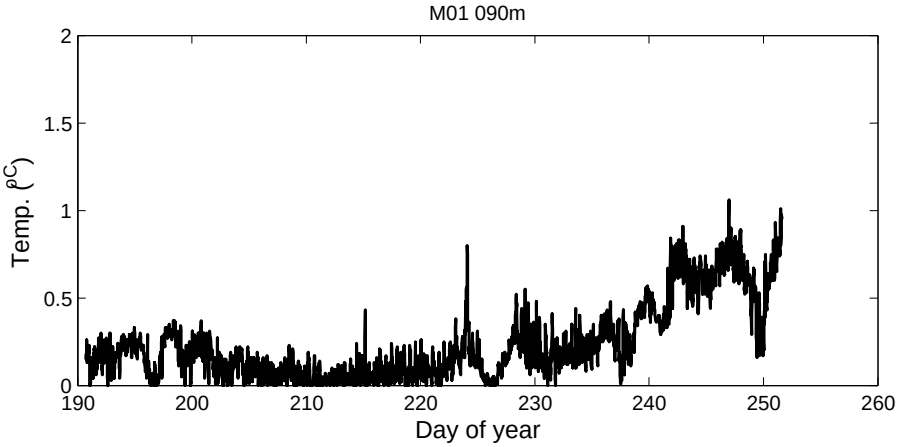

Figure 3.22: Time series plot of thermistors records at 90 m, M1.

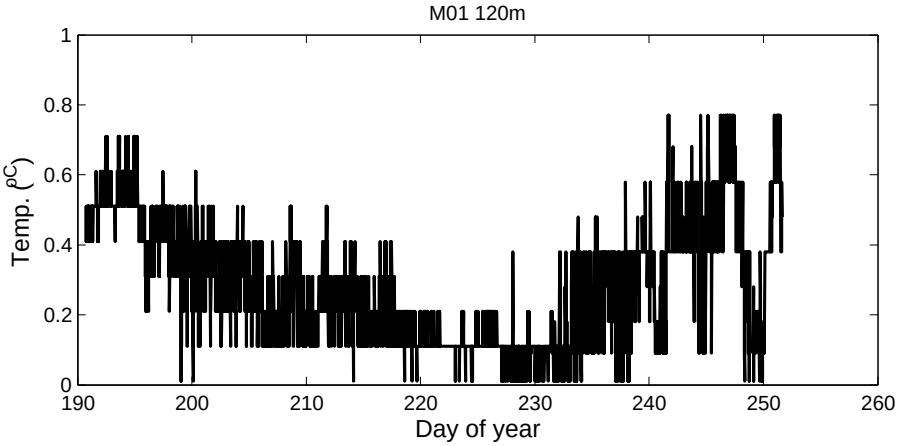

Figure 3.23: Time series plot of thermistors records at 120 m, M1.

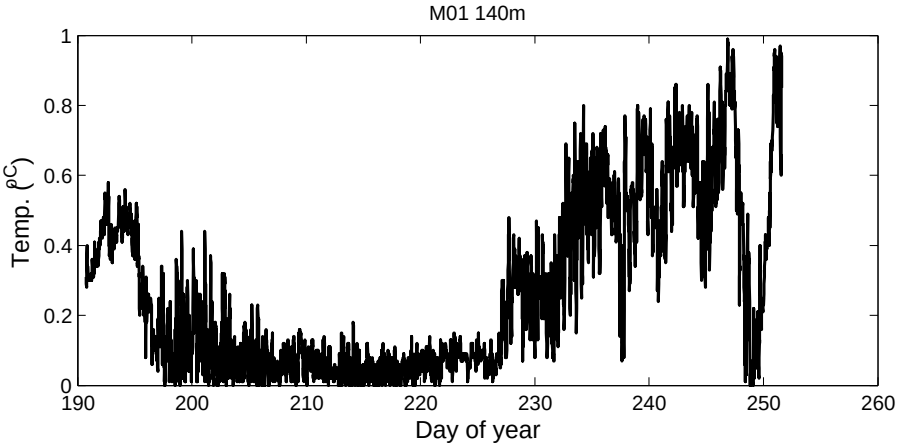

Figure 3.24: Time series plot of thermistors records at140 m, M1.

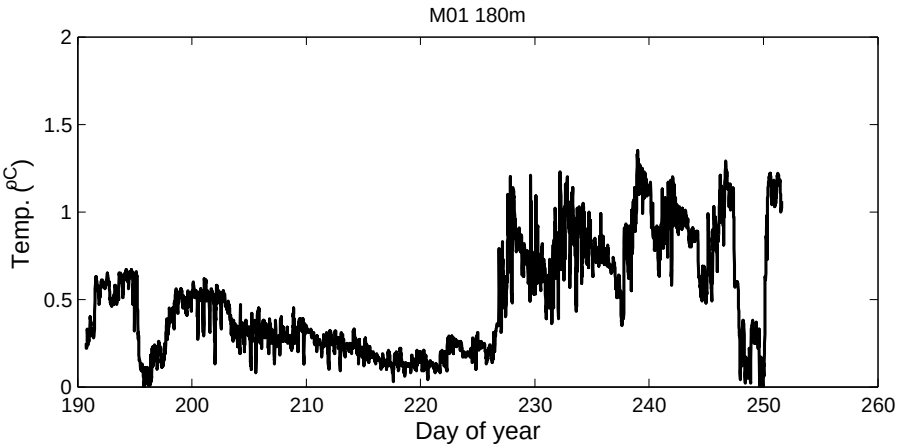

Figure 3.25: Time series plot of thermistors records at 180 m, M1.

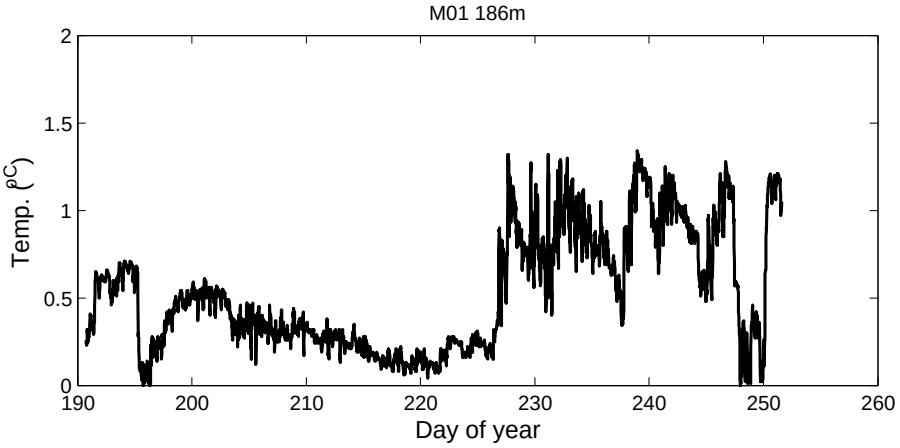

Figure 3.26: Time series plot of thermistors records at 186 m, M1.

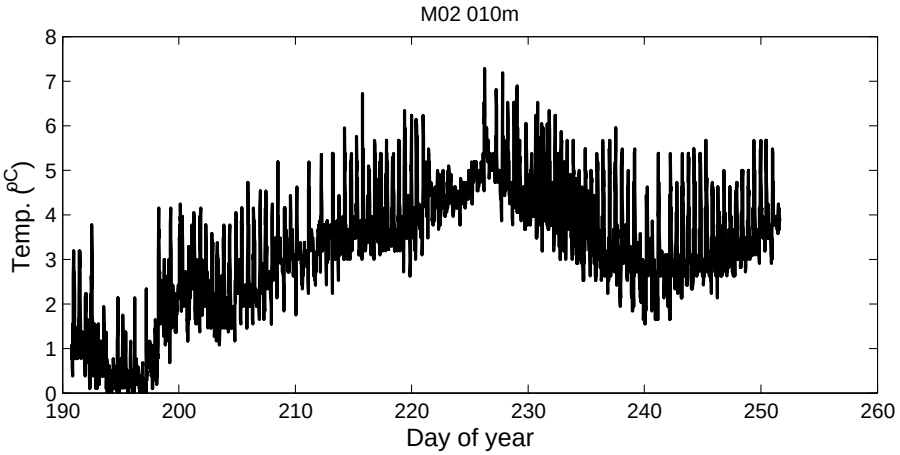

Figure 3.27: Time series plot of thermistors records at 10 m, M2.

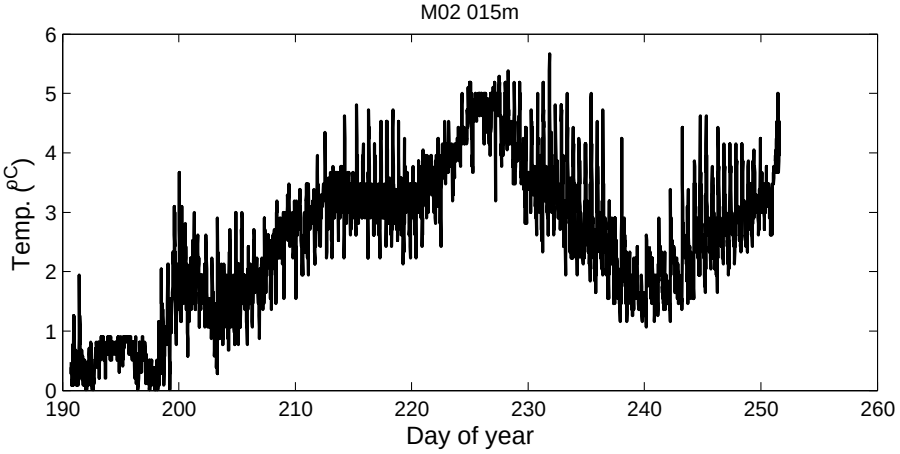

Figure 3.28: Time series plot of thermistors records at 15 m, M2.

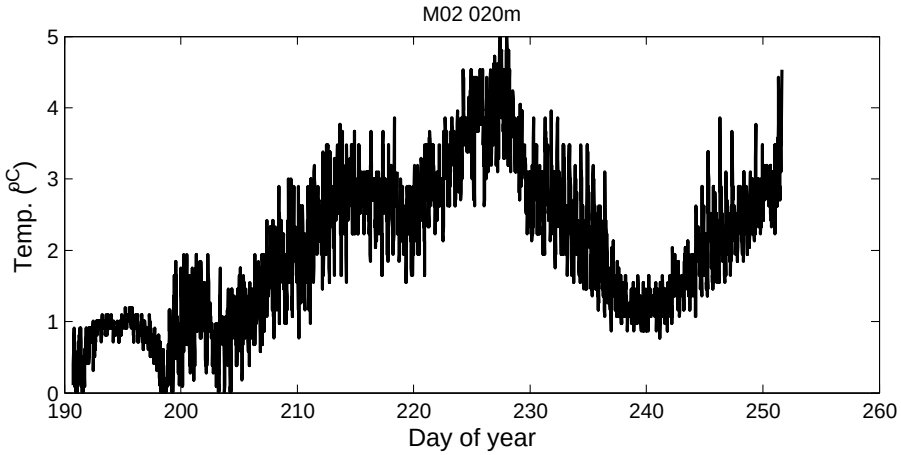

Figure 3.29: Time series plot of thermistors records at 20 m, M2.

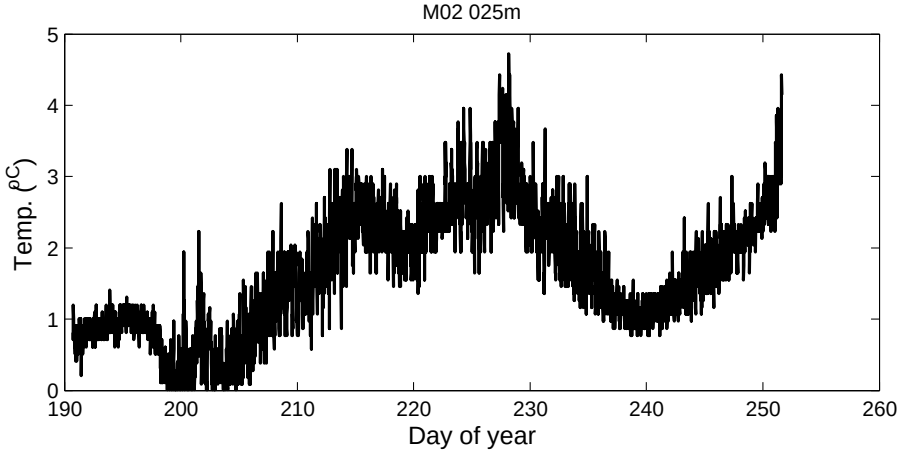

Figure 3.30: Time series plot of thermistors records at 25 m, M2.

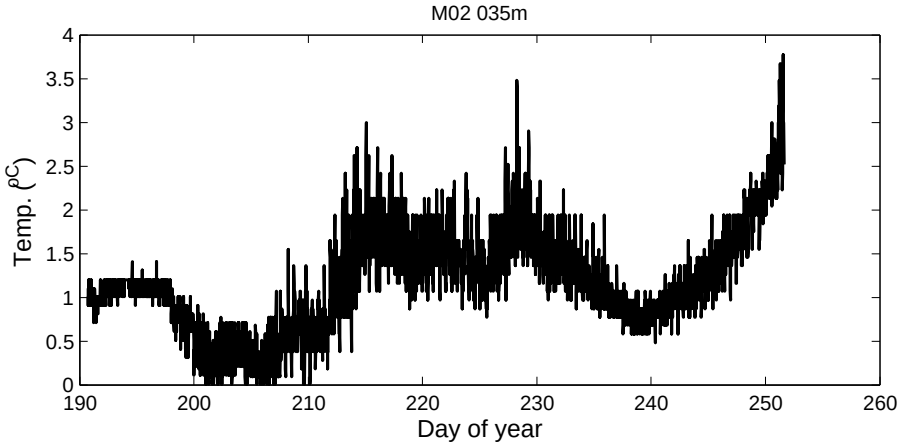

Figure 3.31: Time series plot of thermistors records at 35 m, M2.

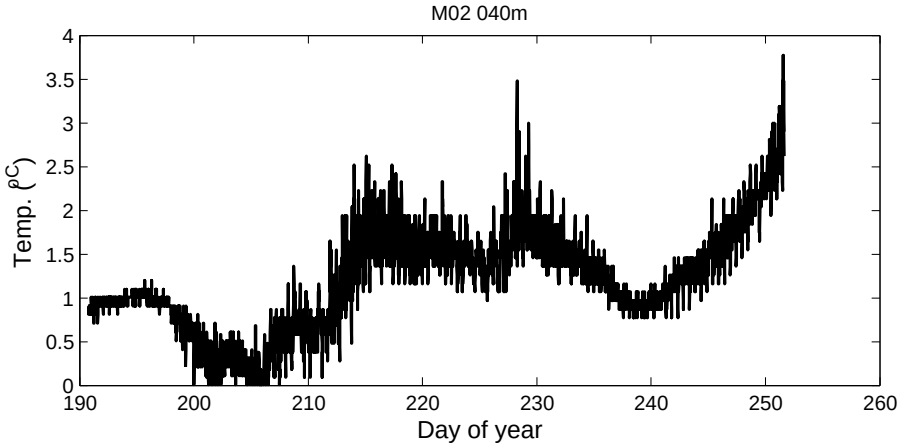

Figure 3.32: Time series plot of thermistors records at 40 m, M2.

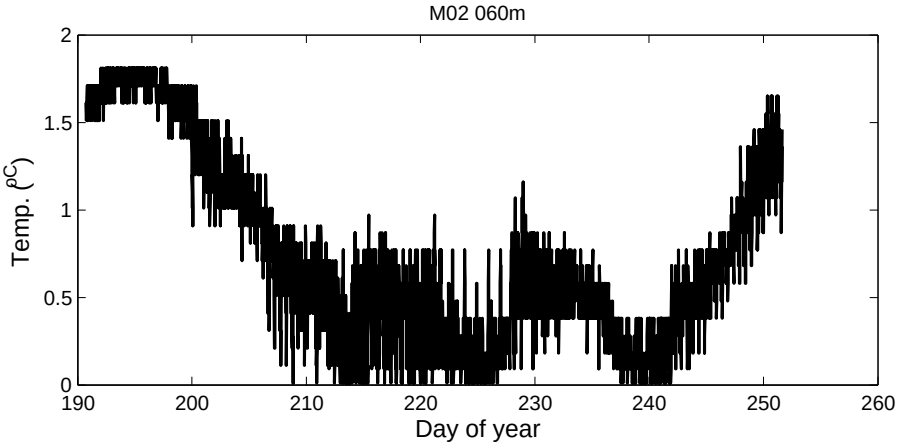

Figure 3.33: Time series plot of thermistors records at 60 m, M2.

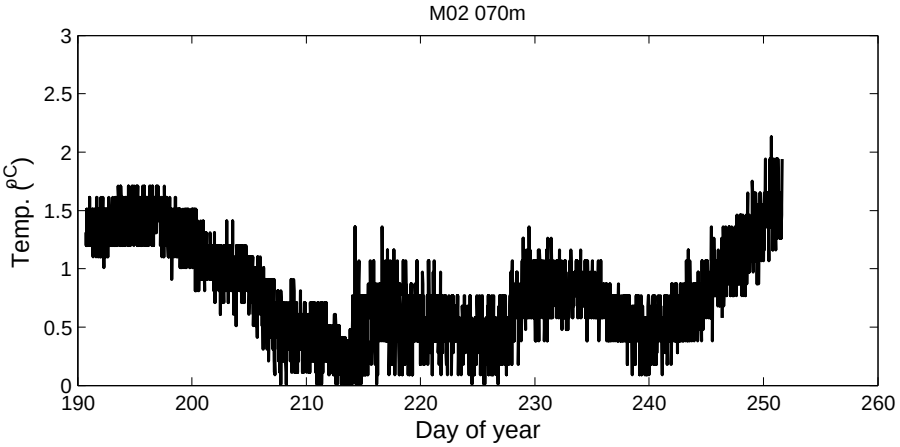

Figure 3.34: Time series plot of thermistors records at 70 m, M2.

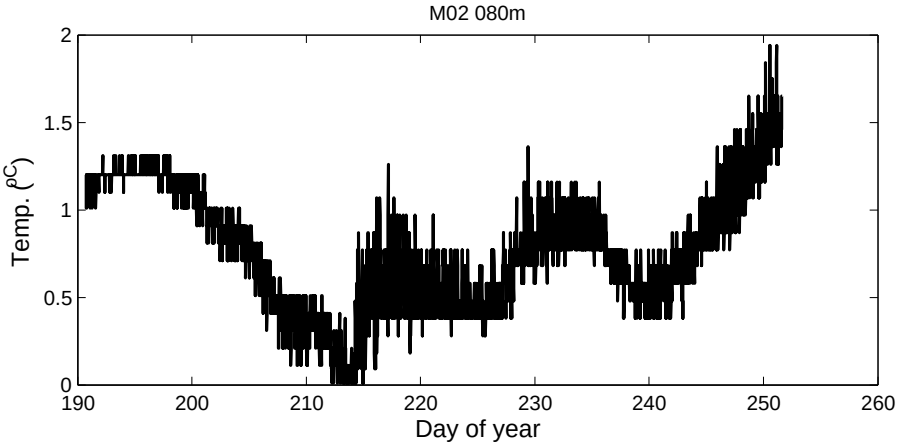

Figure 3.35: Time series plot of thermistors records at 80 m, M2.

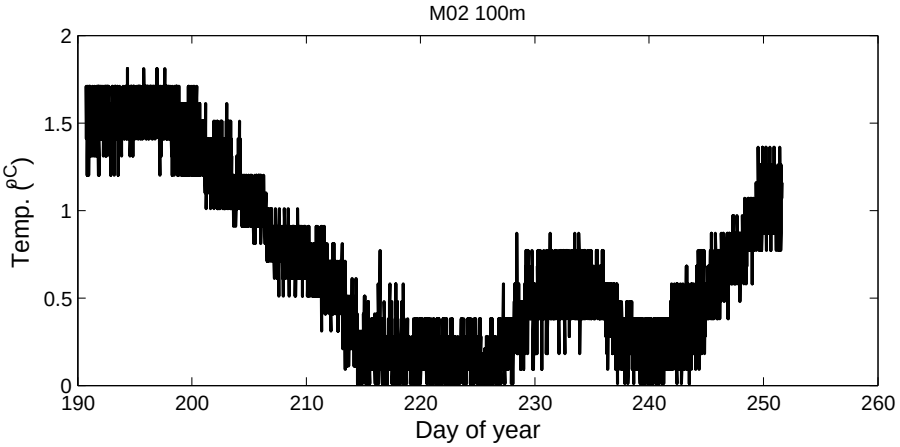

Figure 3.36: Time series plot of thermistors records at 100 m, M2.

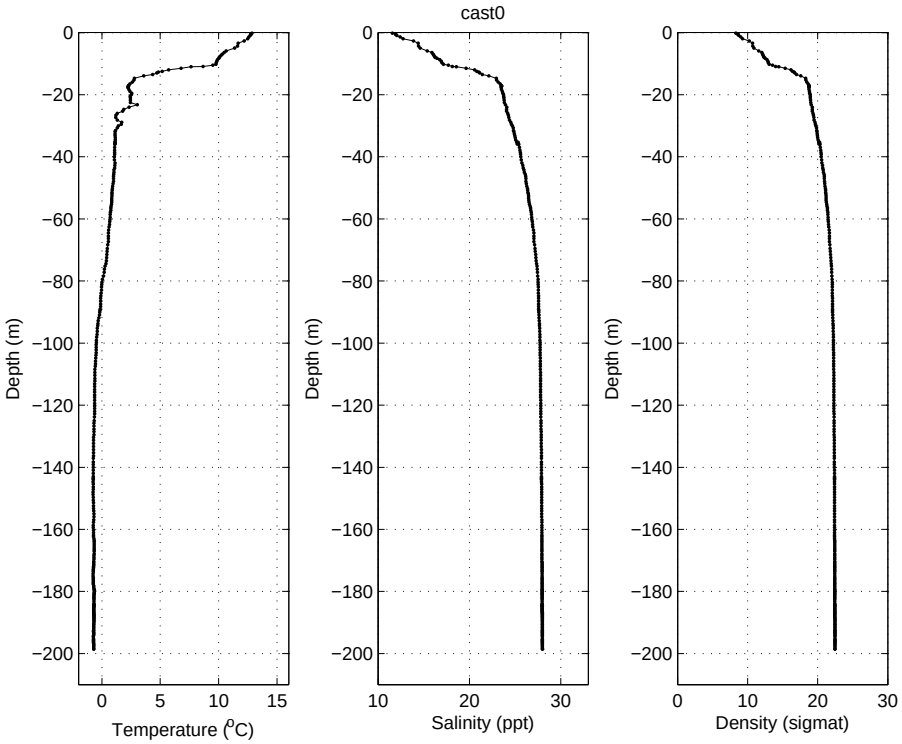

Figure 3.37: Profile of CTD cast number 0.

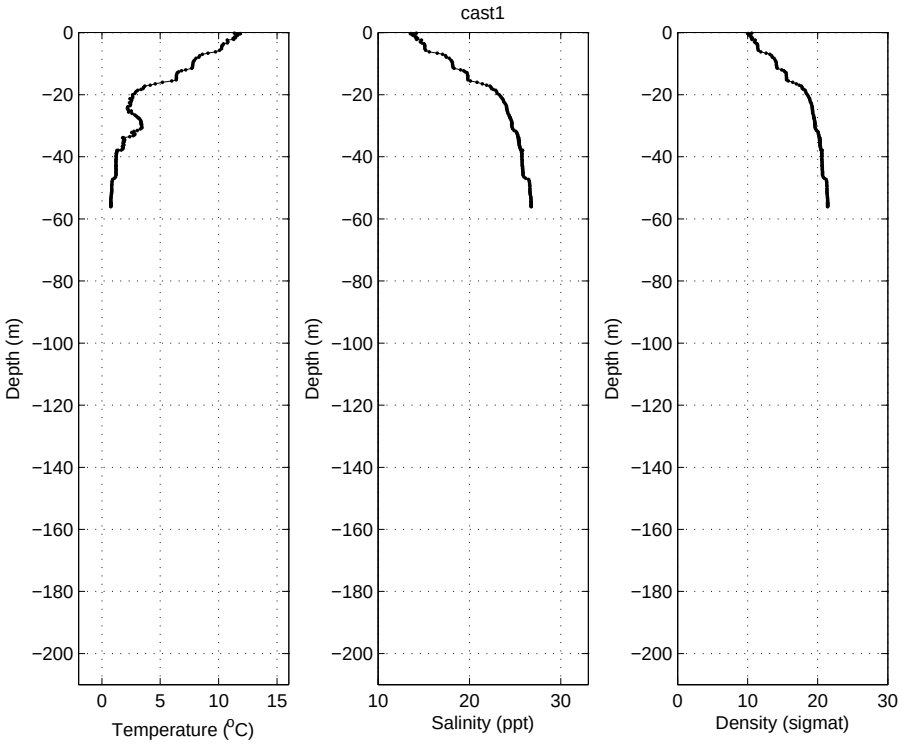

Figure 3.38: Profile of CTD cast number 1.

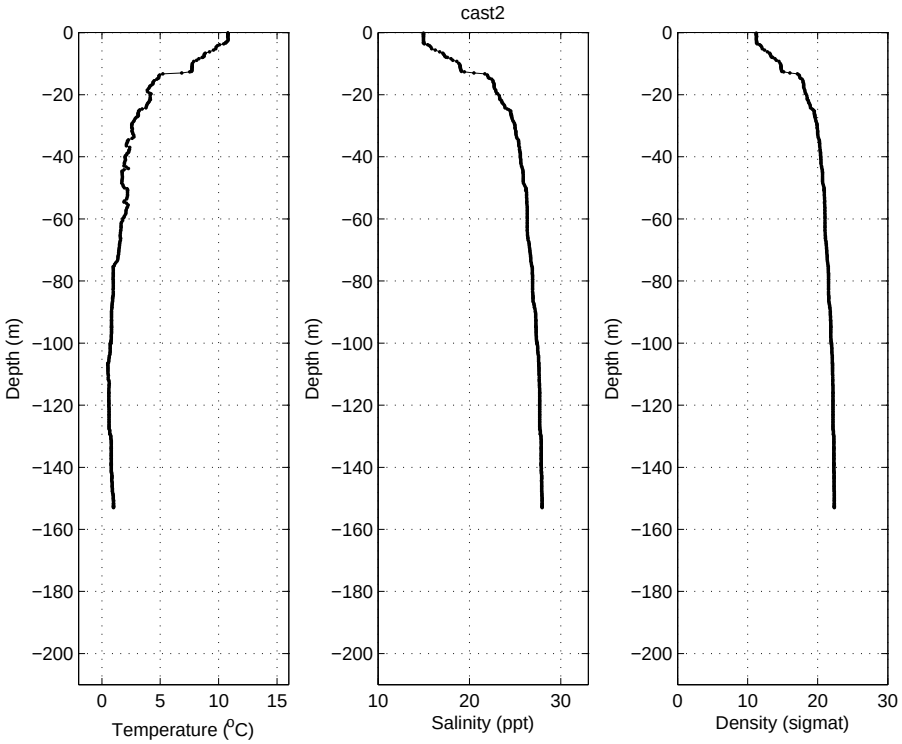

Figure 3.39: Profile of CTD cast number 2.

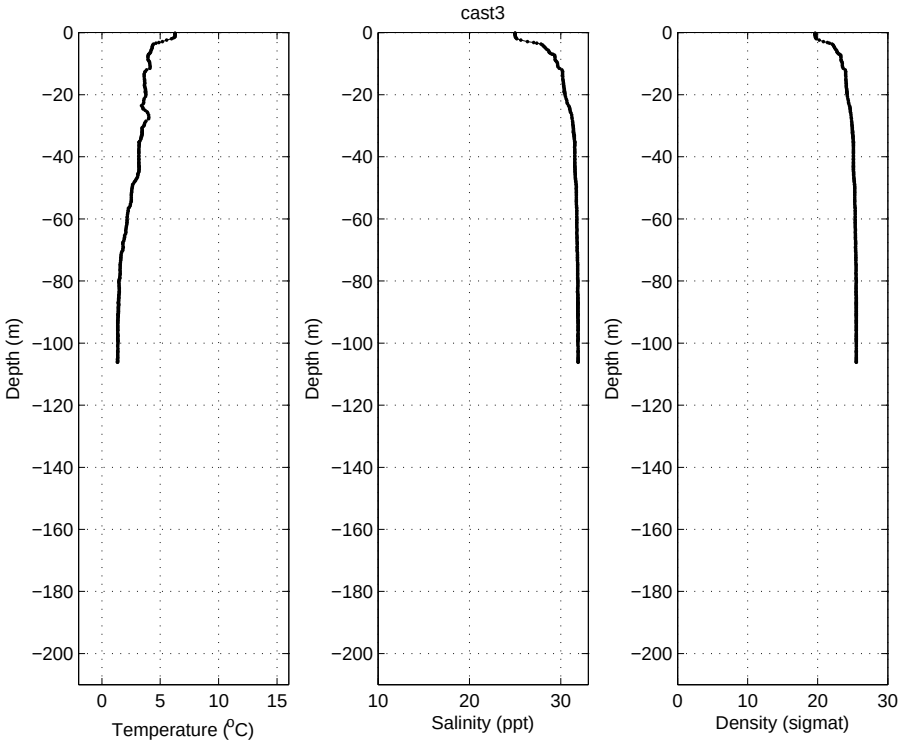

Figure 3.40: Profile of CTD cast number 3.

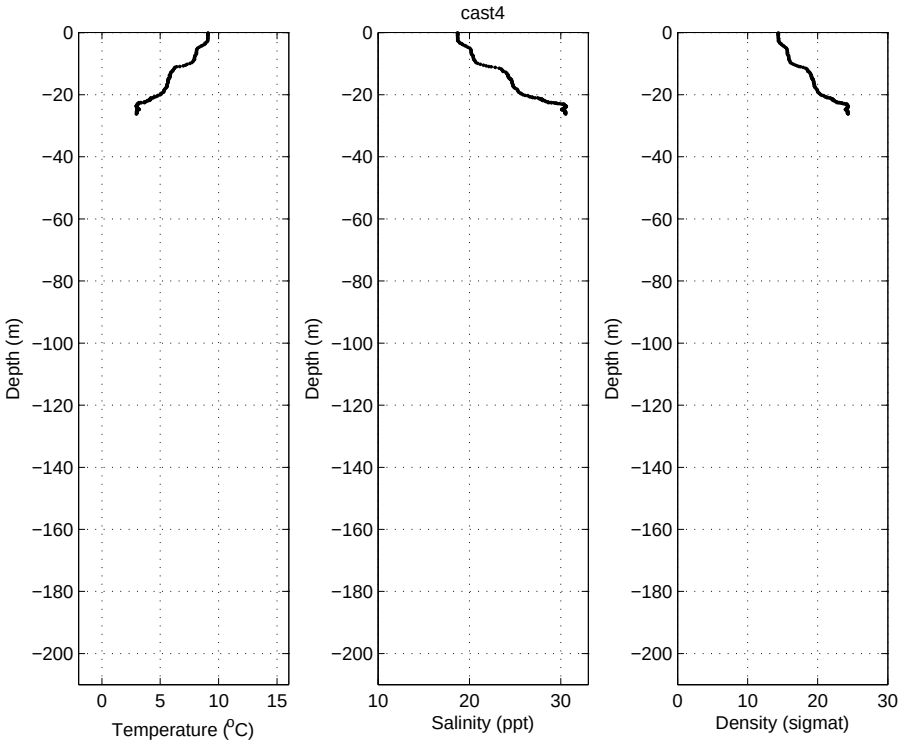

Figure 3.41: Profile of CTD cast number 4.

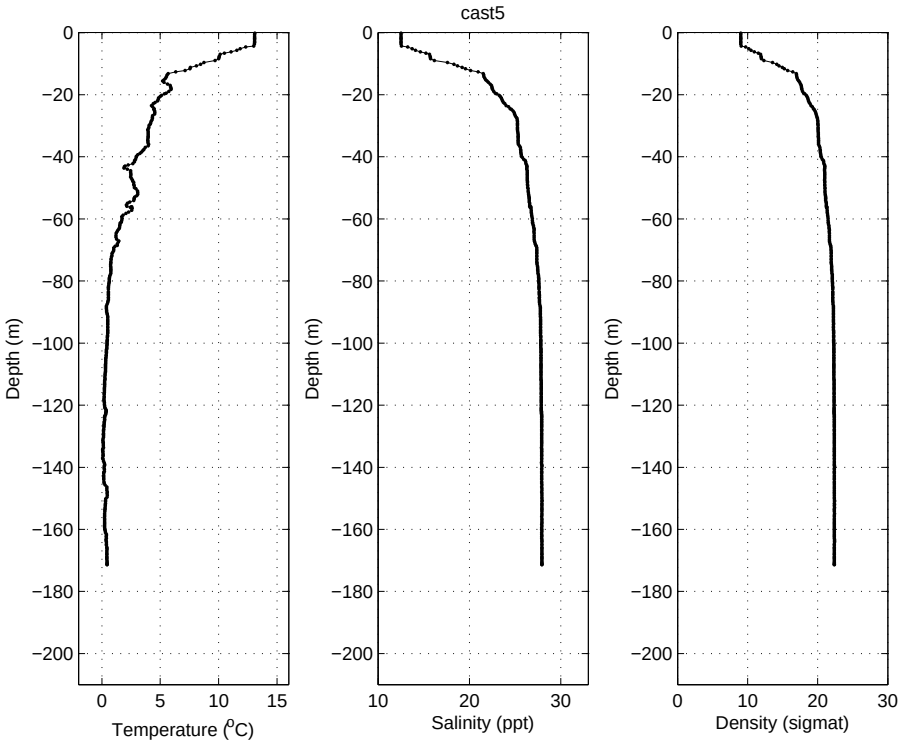

Figure 3.42: Profile of CTD cast number 5.

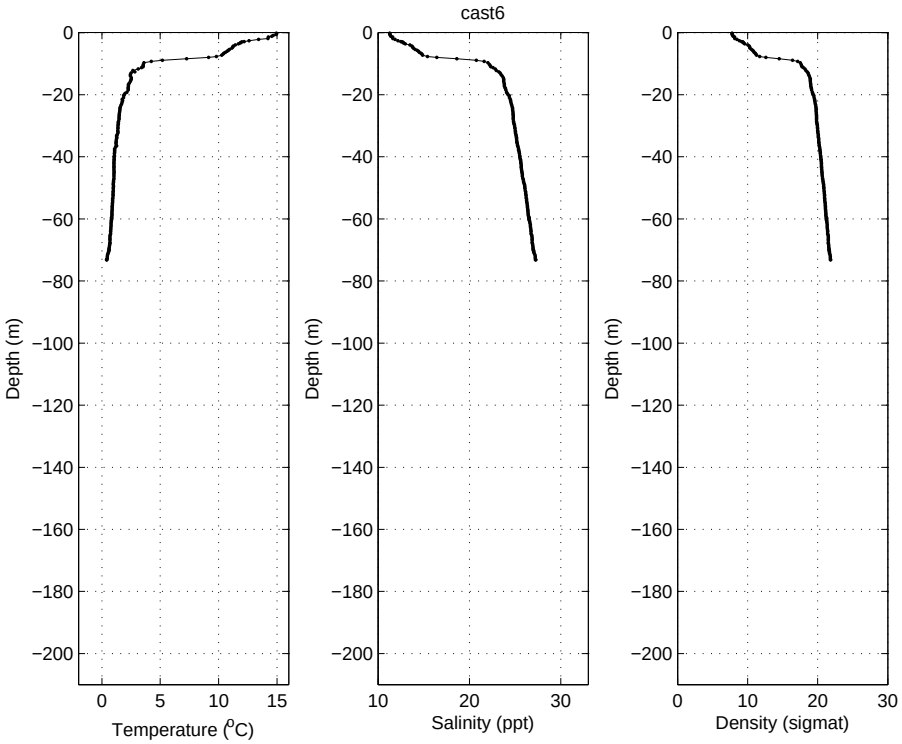

Figure 3.43: Profile of CTD cast number 6.

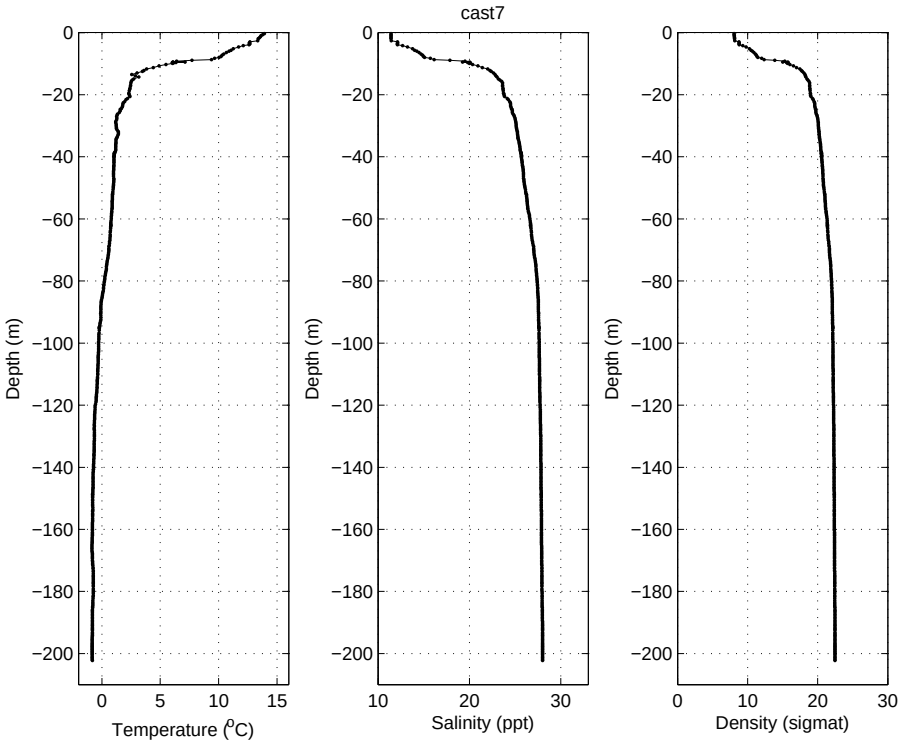

Figure 3.44: Profile of CTD cast number 7.

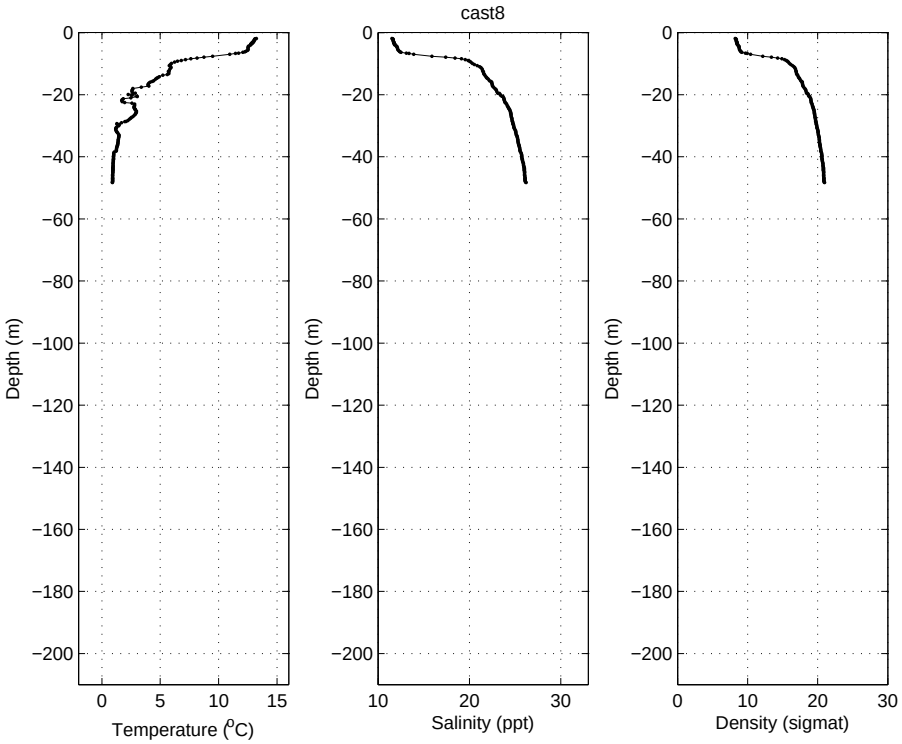

Figure 3.45: Profile of CTD cast number 8.

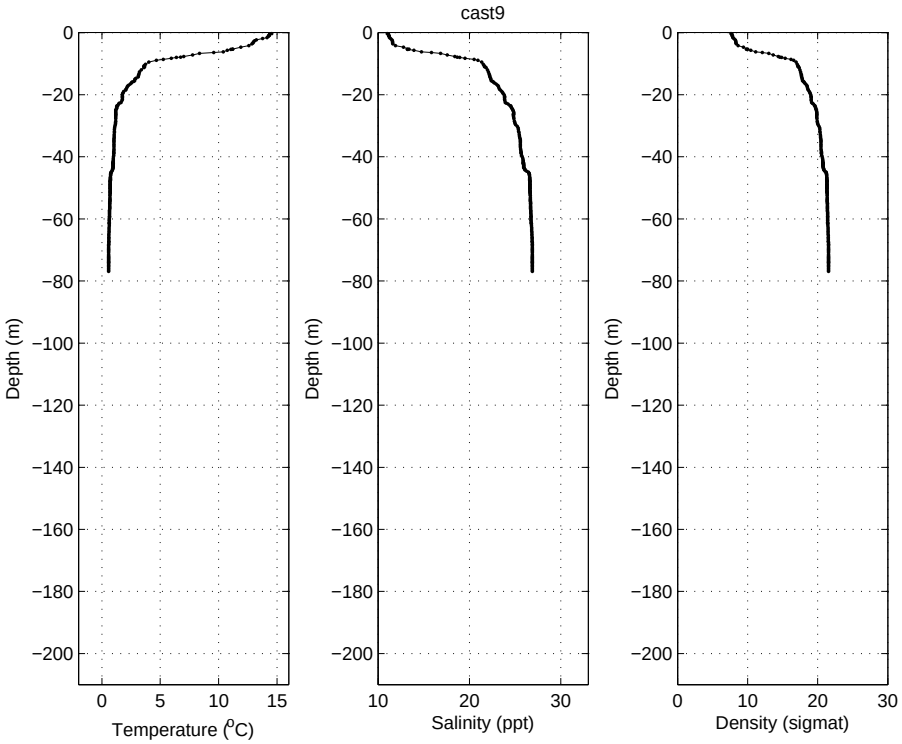

Figure 3.46: Profile of CTD cast number 9.

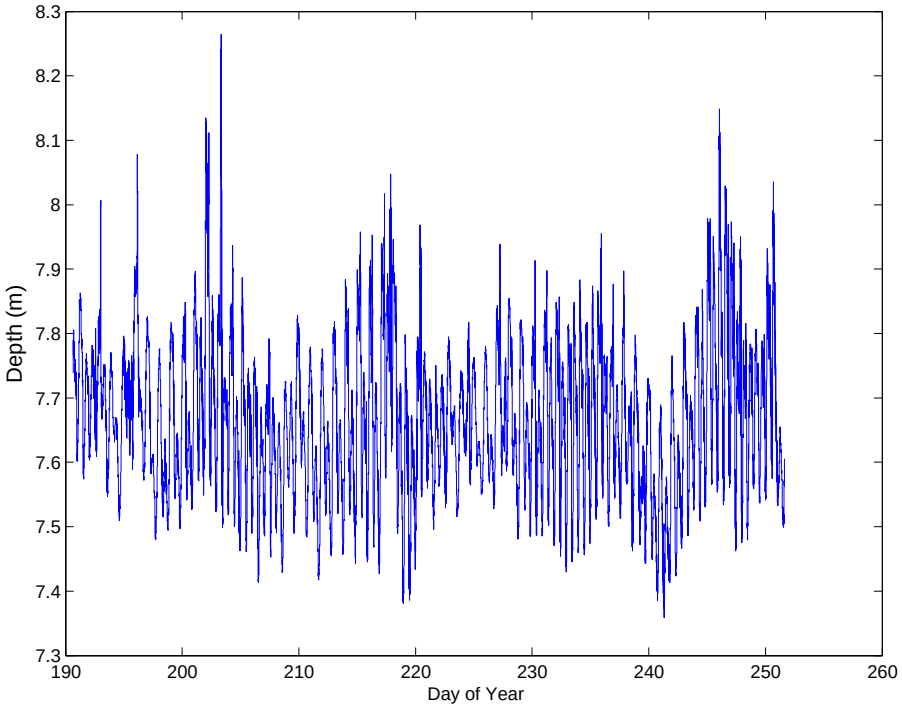

Figure 3.47: Time series plot of pressure records from TDR-2050P Temperature and Depth Logger, M1

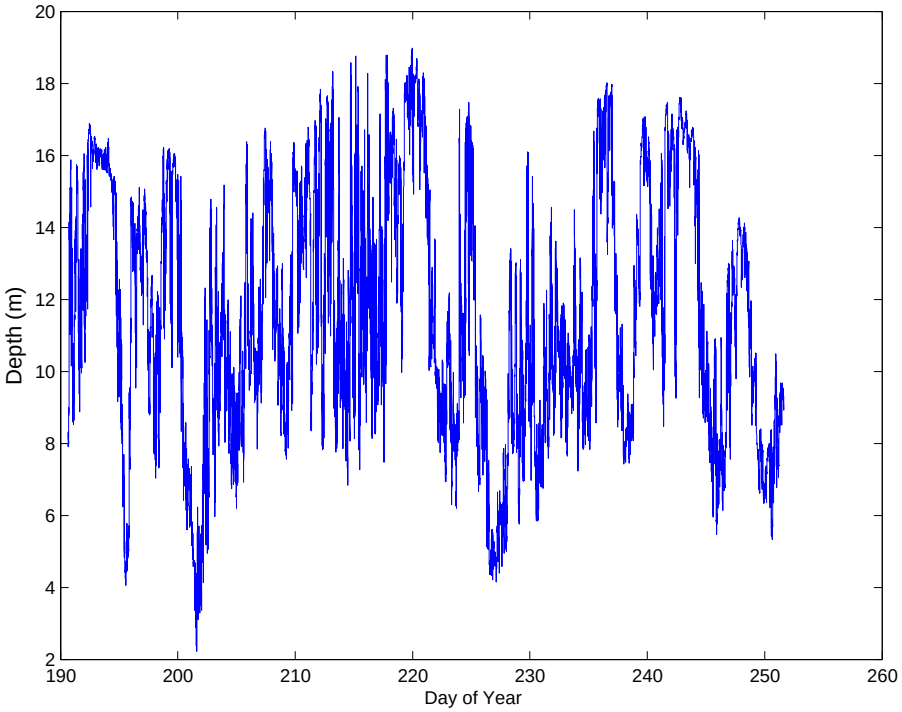

Figure 3.48: Time series plot of temperature records from TDR-2050P Temperature and Depth Logger, M1

Chapter 4

Analysis and Results

Missing or bad data from both the thermistor and ACDP data were dealt with in the same manner: either they were replaced by linearly interpolated values from surrounding points if there was sufficient data, or if there was not, they were removed entirely and omitted from the plots.

Progressive vector plots, were created by calculating the distance travelled at each mooring using the unfiltered velocity data for each 20 minute interval. The position after each day is marked with an x, and the start and end positions are each marked with an unfilled and a filled circle, respectively.

In both the current velocity and the temperature isotherm time series plots , data were filtered using a 5th order forward-and-reverse Butterworth low pass digital filter with a cut-off frequency of 30 hours in order to remove high frequency variability. The filtered data were then interpolated into 0.25 m bins in order to plot the isotherms.

Atmospheric data were obtained from Environment Canada for the same mooring period from the nearby weather monitoring station Happy Valley-Goose Bay. The wind stress calculated from the observed wind speed.

4.1 Statistical analysis

Statistical analysis for temperature, salinity and component velocities were calculated and tabulated (Tables 4.1 and 4.2).

Averaged along Narrows velocity profiles at two mooring stations were calculated by averaging records of each ADCP bin over the mooring time period (Figure 4.1).

At station M1, eastward outflowing water was in the upper 20 m, and the compensating westward inflow was at depth of below 130 m depth. Outgoing eastward current reached its maximum of about 40 cm/s at the surface and

Table 4.1: Summary of current velocities at M1 (unit in cm/s).

		U			V		
Depth	Good Records	Mean	Max	Std. dev.	Mean	Max	Std. dev.
5	4382	38.17	191.10	102.94	10.57	169.90	58.77
11	4387	9.97	71.10	30.74	3.29	53.70	20.41
15	4381	2.73	67.20	17.87	3.51	44.10	10.79
21	4138	1.53	-78.30	15.41	1.48	63.00	10.87
31	4361	0.87	80.60	14.15	0.64	52.60	10.81
51	4389	1.95	57.00	14.12	1.12	51.10	10.69
75	4389	2.19	39.40	13.78	1.99	33.20	10.32
101	4389	0.68	33.20	11.72	0.71	-27.90	9.31
125	4389	-0.93	36.70	11.59	-1.60	-36.50	9.05
151	4389	-5.09	-51.80	12.38	-4.29	-45.60	9.71
175	4176	-8.51	-62.20	13.47	-5.65	-49.90	12.15
201	4376	-0.16	12.90	0.96	-0.14	8.30	0.96

Table 4.2: Summary of current velocities at M2 (unit in cm/s).

		U			V		
Depth	Good Records	Mean	Max	Std. dev.	Mean	Max	Std. dev.
4	3885	28.97	328.90	48.09	8.51	180.80	26.54
10	4314	44.47	301.20	73.21	15.01	171.90	33.01
14	4017	12.90	168.80	30.87	5.47	124.70	19.82
20	3629	11.61	95.90	30.71	8.22	81.10	14.48
30	3633	-5.17	-119.10	28.06	1.79	-136.40	9.51
50	3662	-11.11	-97.00	27.20	-2.52	58.80	10.54
74	3911	-13.35	-102.10	29.54	-2.57	-38.80	9.98
100	4421	-13.89	-99.40	29.11	-3.86	-39.60	12.03

decreased to zero around 20 m depth. Inflow westward current reached a maximum of about 10 cm/s at the 180 m depth. The averaged speed between 20 m and 130 m was very weak.

At station M2, the estuarine circulation is clearly shown, with eastward water in the upper 30 m, and the compensating westward inflow below 30 m depth. Averaged outgoing speed is about 20 cm/s at the surface and gradually increased to its maximum of about 50 cm/s at 10 meter depth. The speed then decreed with depth and changed direction to inward at depth of 30 m. Between depth 40 m to bottom, inward speed are changed gradually around 12 cm/s. It appeared that the velocity profile shown at mooring M2 is volume conserving.

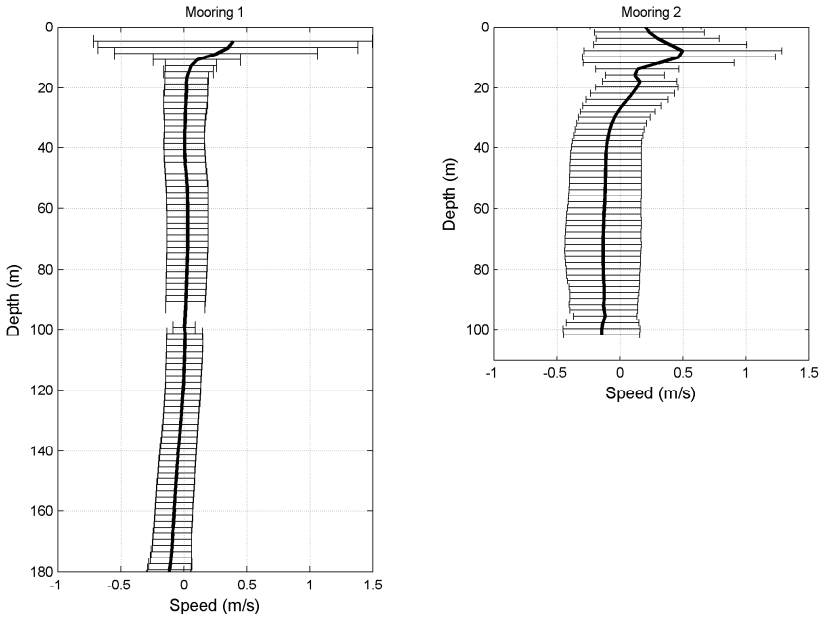

Figure 4.1: Averaged along Narrows velocity profile at M1 and M2 stations.

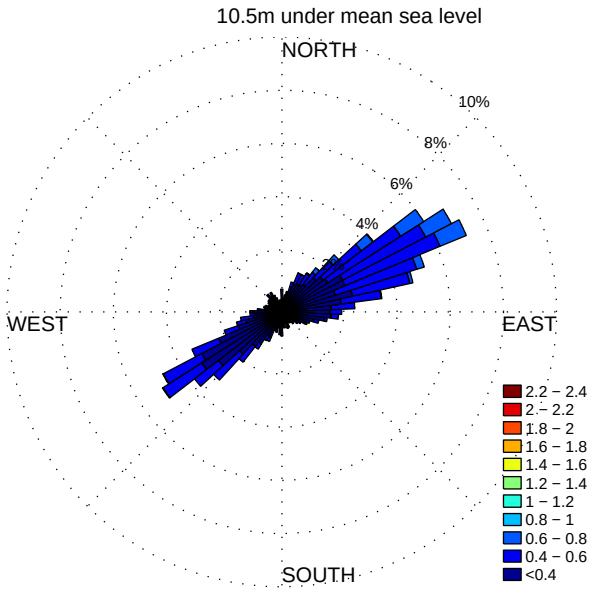

Figure 4.2: Rose plots of current at 11 m depth, M1 station.

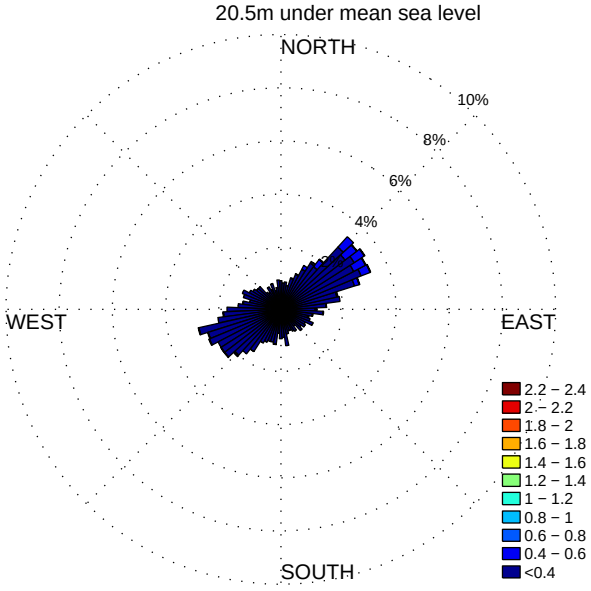

Figure 4.3: Rose plots of current at 21 m depth, M1 station.

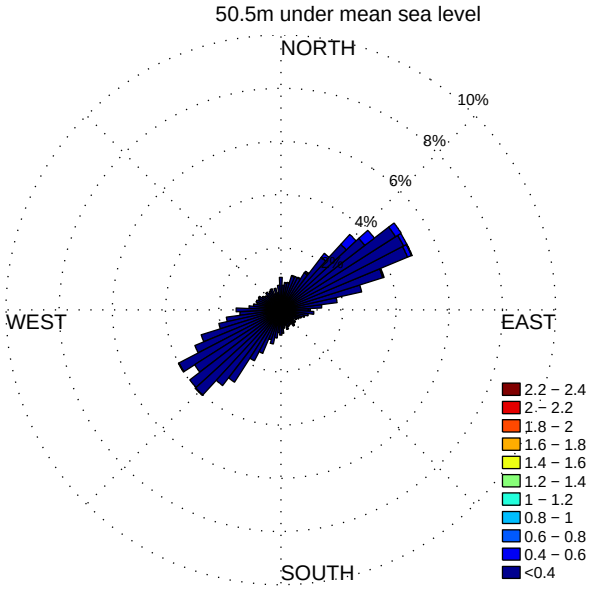

Figure 4.4: Rose plots of current at 51 m depth, M1 station.

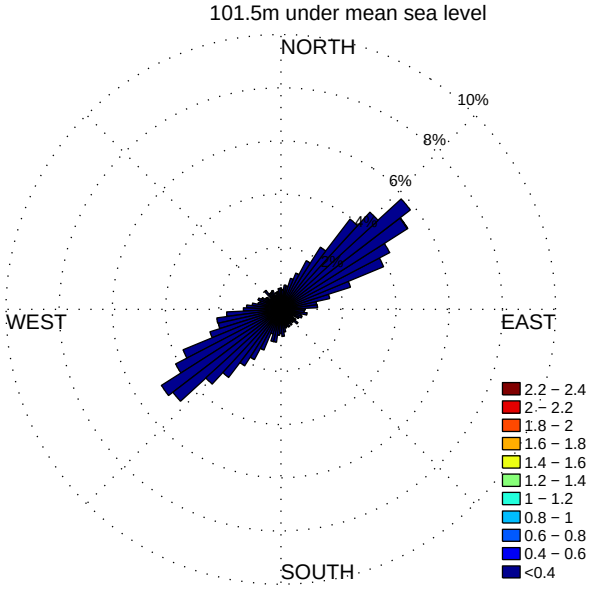

Figure 4.5: Rose plots of current at 101 m depth, M1 station.

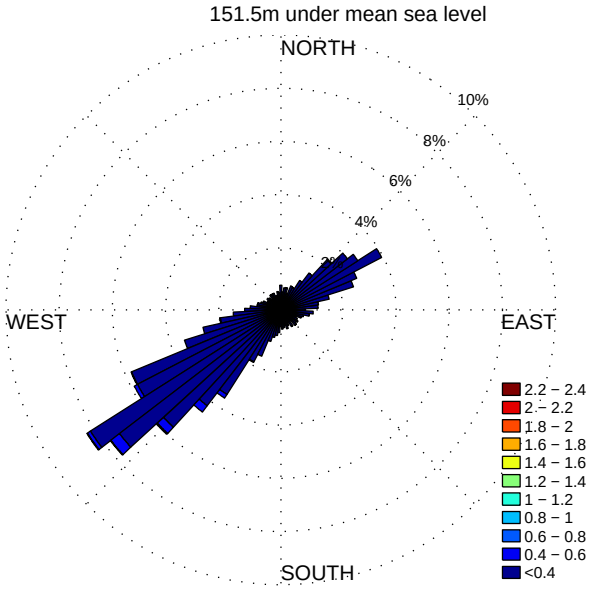

Figure 4.6: Rose plots of current at 151 m depth, M1 station.

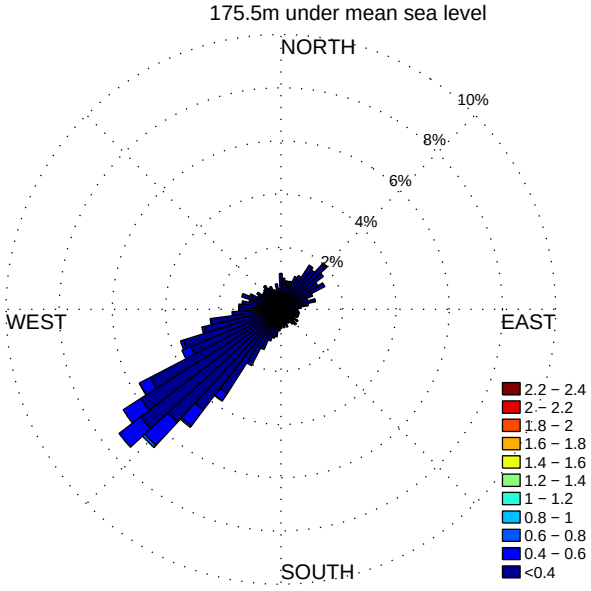

Figure 4.7: Rose plots of current at 175 m depth, M1 station.

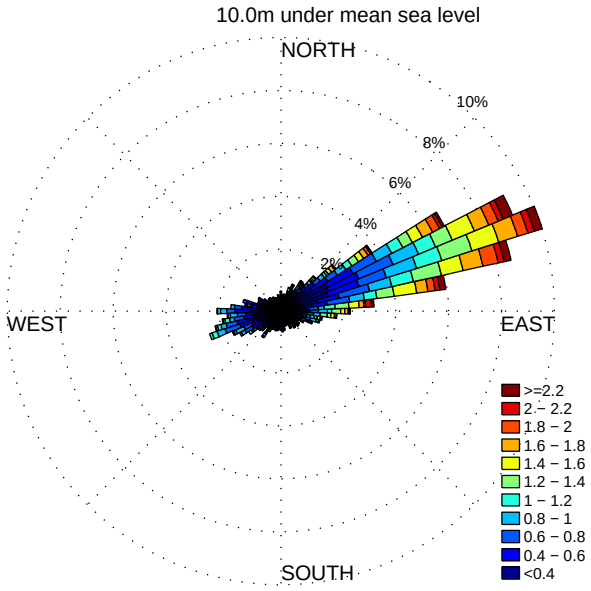

Figure 4.8: Rose plots of current at 10 m depth, M2 station.

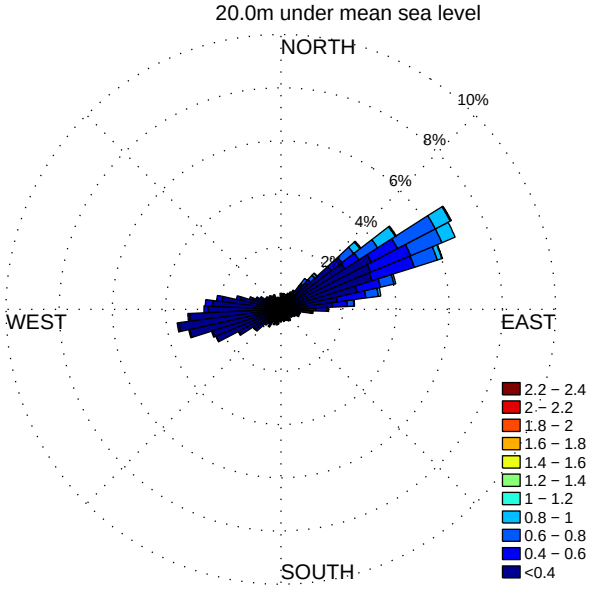

Figure 4.9: Rose plots of current at 10 m depth, M2 station.

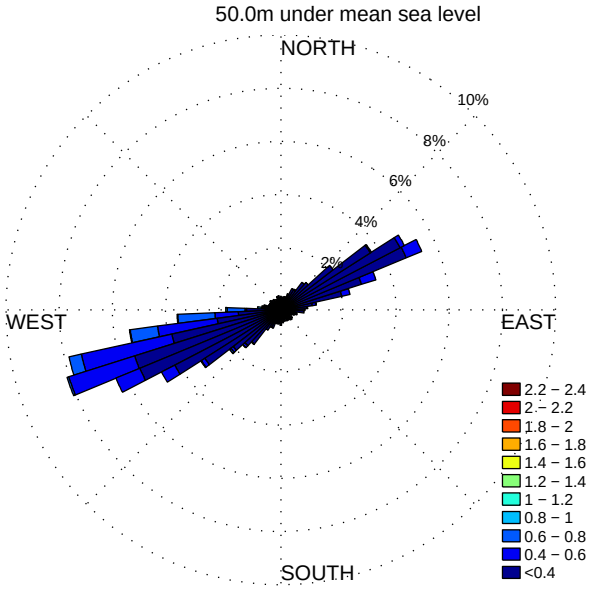

Figure 4.10: Rose plots of current at 50 m depth, M2 station.

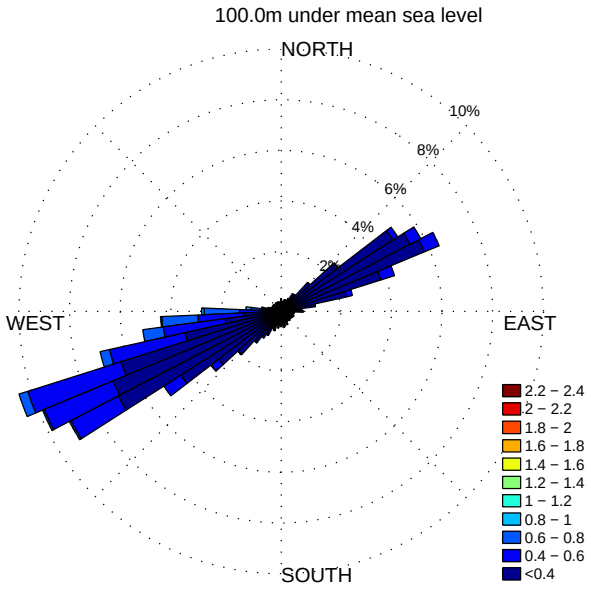

Figure 4.11: Rose plots of current at 100 m depth, M2 station.

4.2 Current rose

Rose plots for currents are presented in this section to show the current direction and percentage frequency of speed in specific intervals. The rose plots in Figures 4.2 and 4.11 give details of the described pattern of flood and ebb circulation for the two moorings. The overall rose plots show that there are clearly preferred current direction roughly along the narrows for both mooring locations. This significant symmetry in current direction also indicates that falling tide was in an opposite direction to rising tide.

At mooring M1, the currents flowed along the axis of the fjord towards and away from the Narrows (Figures 4.2 - 4.40). Near the surface at about 10 m depth, the prevalent direction was outward. Near the bottom, the flow direction was mainly inward. This symmetry of directions between ebb and flood tides indicates an strong and regular tidal signal. During the flood phase, the tidal current near the surface are enough to overcome the eastward outflow, and enhance the inflow at depth. During an ebb tidal phase, the surface average flow is out of the bay but the current at 175 m depth is still inward.

At mooring M2, it shows that currents flowed in dominant directions of along the narrows as well(Figures 4.8 - 4.11). At the surface, the flow was in outward direction both during flood and ebb tidal phases. Near the bottom, there is a symmetry between ebb and flood tidal current directions, and the prevailing direction was inward.

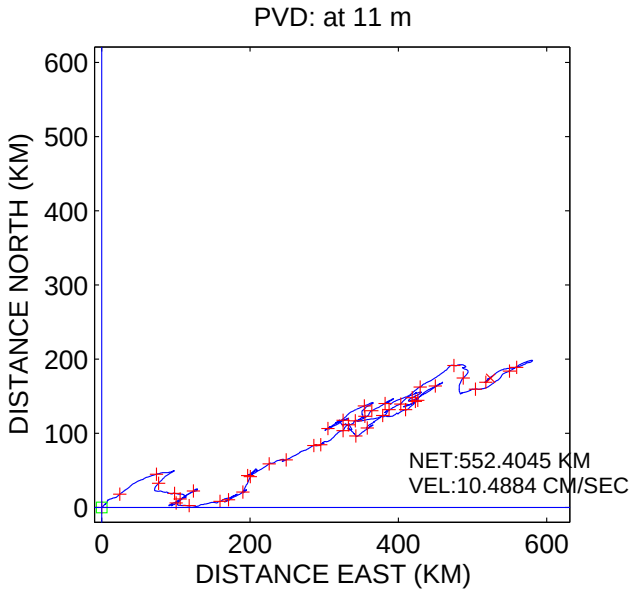

Figure 4.12: Progressive vector diagrams at 11 m depth, M1 station.

4.3 Progressive vector diagrams

Progressive vector diagrams show the distance and direction a particle of water would travel if the flow were spatially uniform. The progressive diagrams in Figures 4.12 - 4.21 were produced from 20-minute samples. The cross marks in the diagram represent time intervals of two days. Variabilities of different timescales are superimposed on the residual current according to the progressive vector diagrams. A net displacement in outward direction at the surface and an inward flow near the bottom can be found at both mooring stations.

At mooring M1, averaged surface current velocity was 39 cm/s over the duration of the measurements. At the depth of 21 m, substantial variability in velocity direction is present and the averaged speed reduced to only 2 cm/s. A very organized flow was found at depth of 175 m and the inward flow reached its maximum speed of 10 cm/s.

At mooring M2, the averaged outward current at 10 m depth was 46 cm/s and directional variability was weak. At 50 m depth, the averaged current direction switched from northeast to southwest anticlockwise. At the depth of 100 m, current direction was very organized and increased to 14 cm/s.

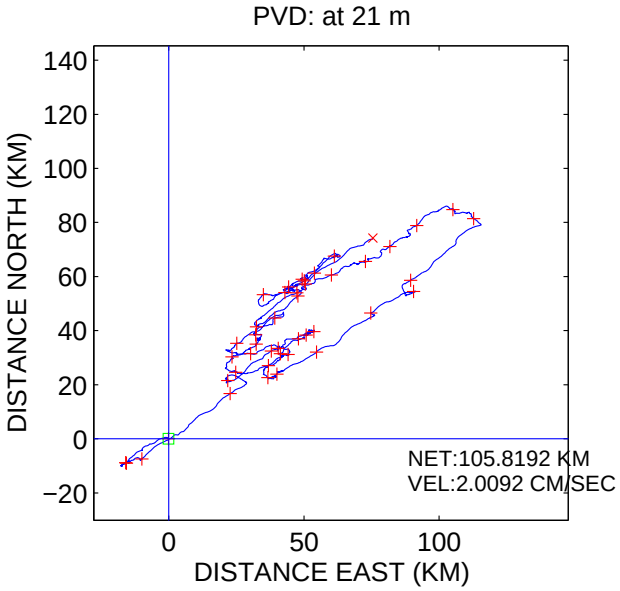

Figure 4.13: Progressive vector diagrams at 21 m depth, M1 station.

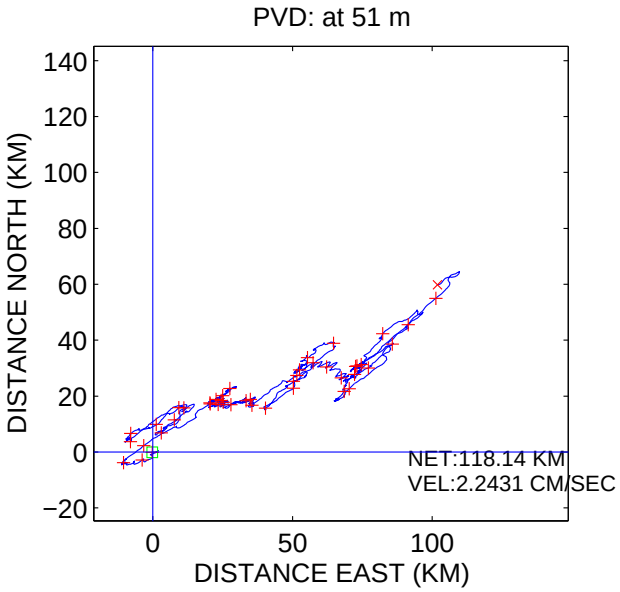

Figure 4.14: Progressive vector diagrams at 51 m depth, M1 station.

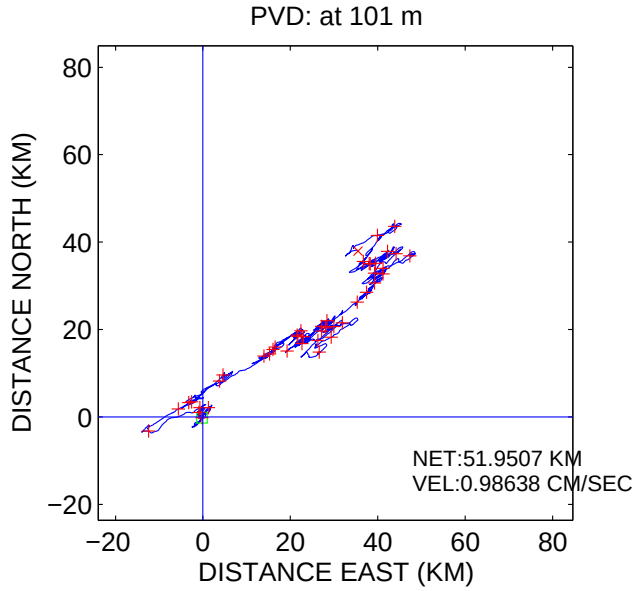

Figure 4.15: Progressive vector diagrams at 101 m depth, M1 station.

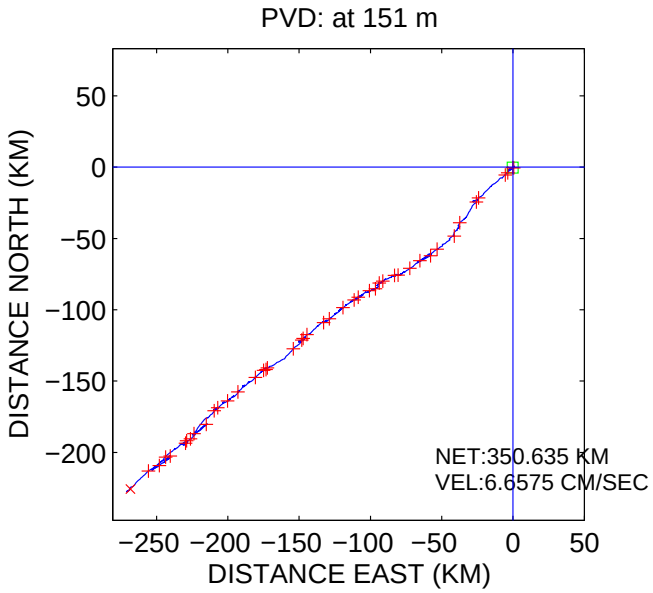

Figure 4.16: Progressive vector diagrams at 151 m depth, M1 station.

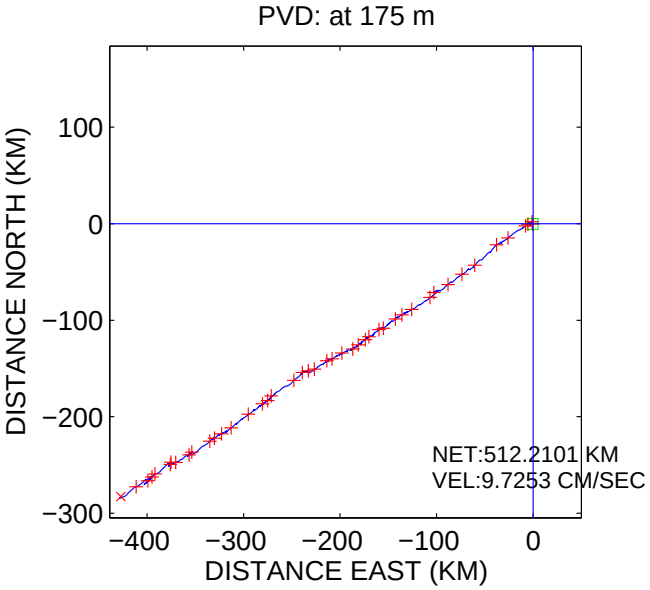

Figure 4.17: Progressive vector diagrams at 175 m depth, M1 station.

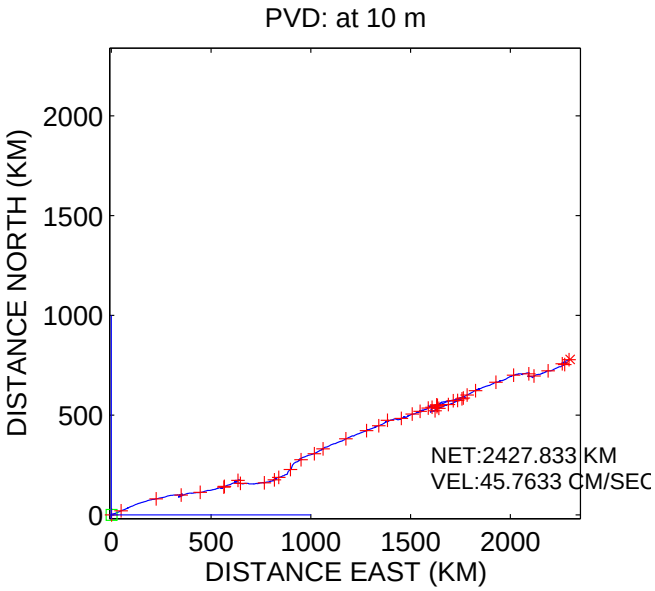

Figure 4.18: Progressive vector diagrams at 10 m depth, M2 station.

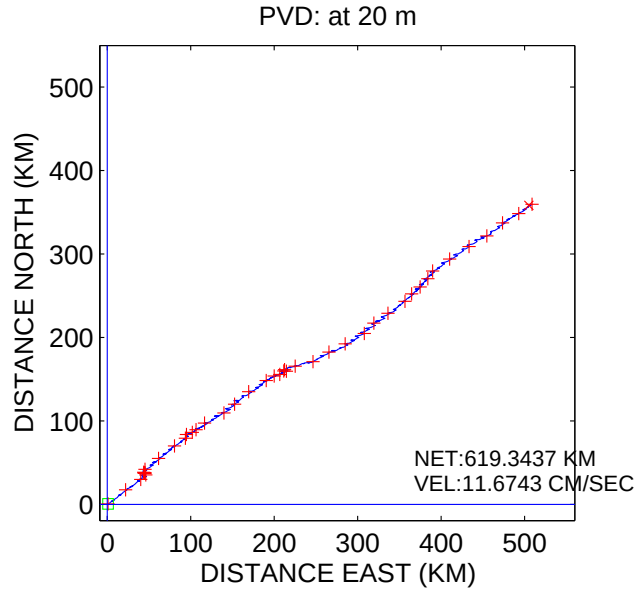

Figure 4.19: Progressive vector diagrams at 10 m depth, M2 station.

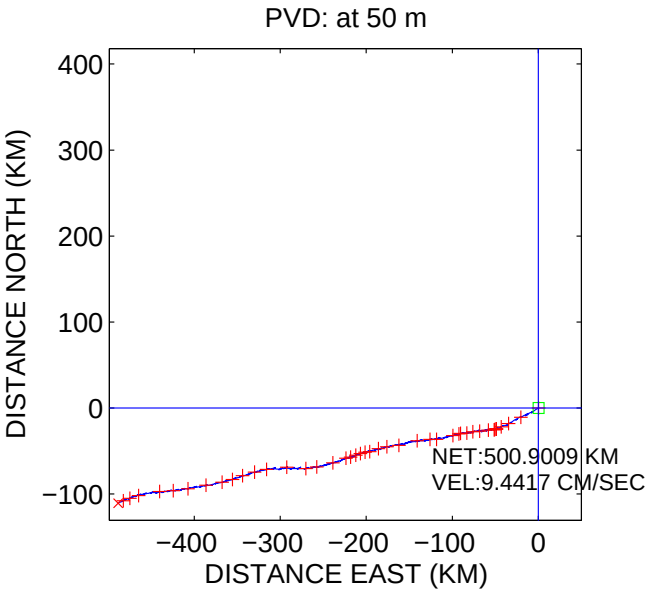

Figure 4.20: Progressive vector diagrams at 50 m depth, M2 station.

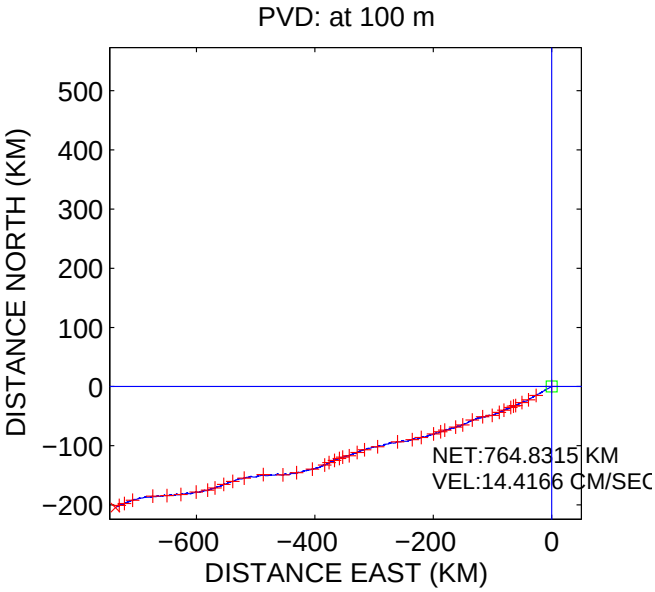

Figure 4.21: Progressive vector diagrams at 100 m depth, M2 station.

4.4 Spectral Analysis

Spectral analysis was used to investigate the kinetic energy distribution. The current data series were decomposed into their East-West component, U and North-South component, V. The Power Spectral Density technique was performed on each of them separately.

Figures 4.22- 4.31 show graphically, the results of the spectral calculations for both the U and V components of selected depth at both mooring stations. The Power Spectral Density plots indicate that a low frequency current with a period longer than 2 days (0.5 cpd) and K_1 were the most significant current at the surface. Below the outward surface flow, it shows that the semidiurnal tides (M_2) dominate the energy spectrum for both locations. Inertial current (about 16 hours period) was found not important to the energy spectrum. The meridional (North/South) component was found weaker than the zonal component (East/West).

4.5 Harmonic Analysis

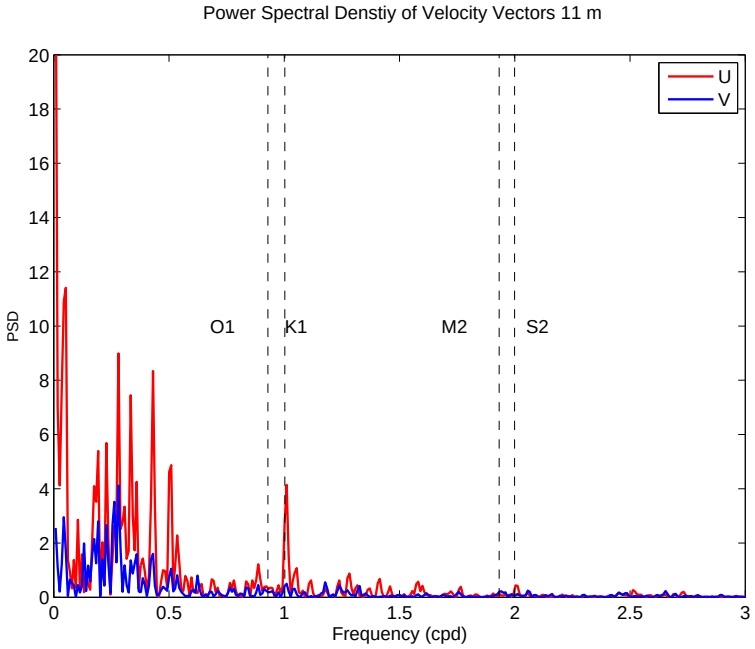

Figure 4.22: Power Spectral Density plot at 11 m, M1.

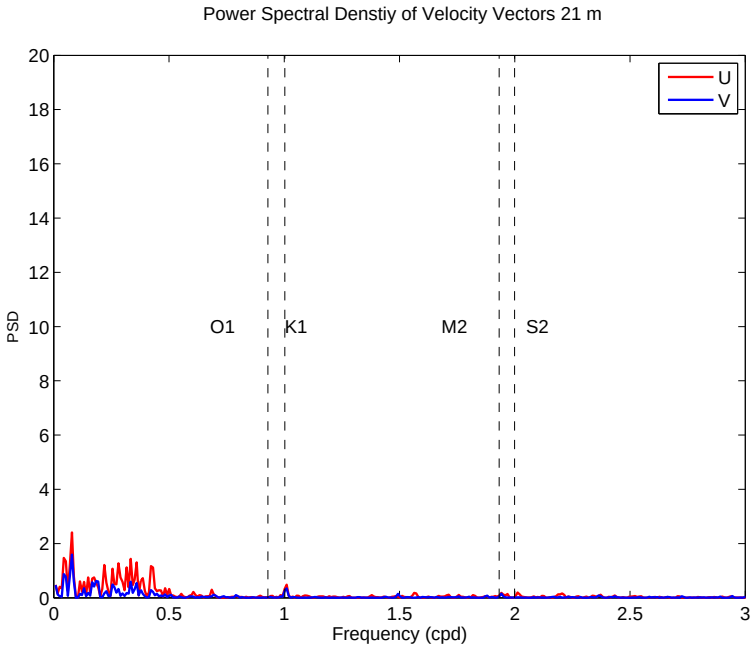

Figure 4.23: Power Spectral Density plot at 21 m, M1.

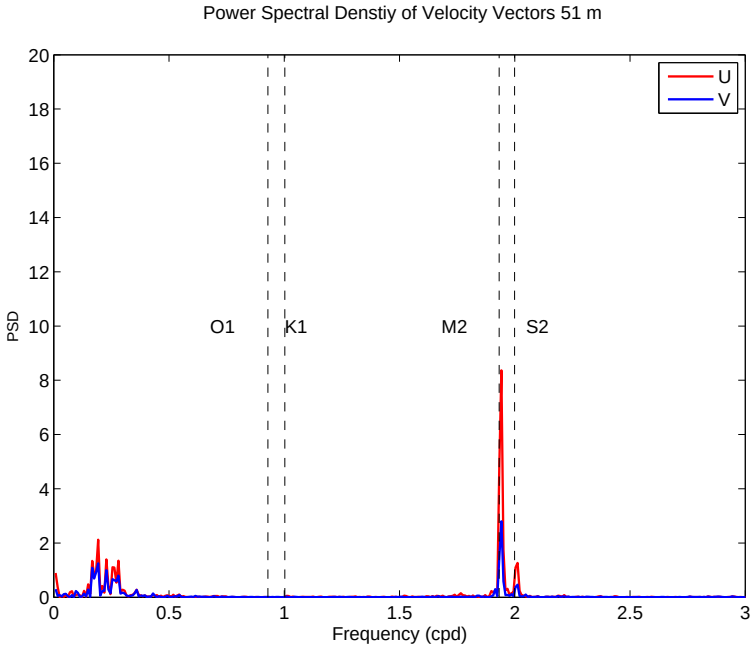

Figure 4.24: Power Spectral Density plot at 51 m, M1.

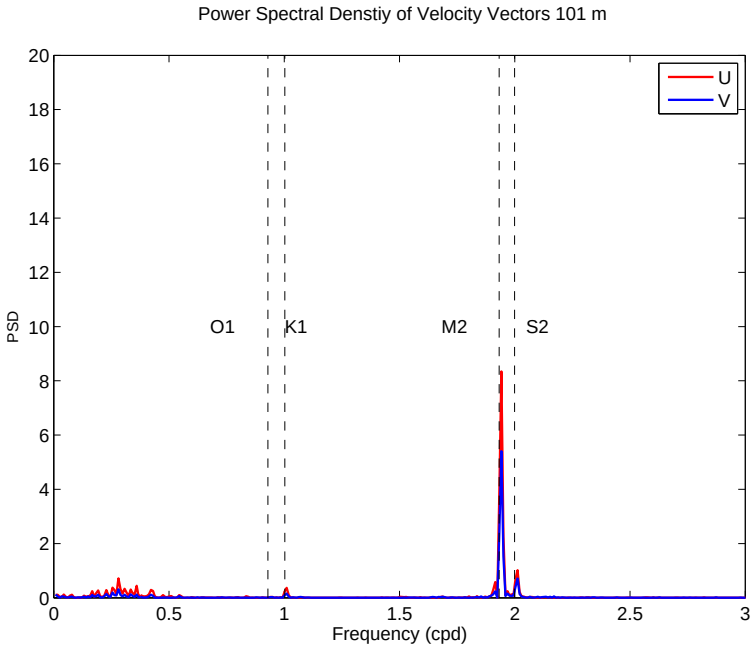

Figure 4.25: Power Spectral Density plot at 101 m, M1.

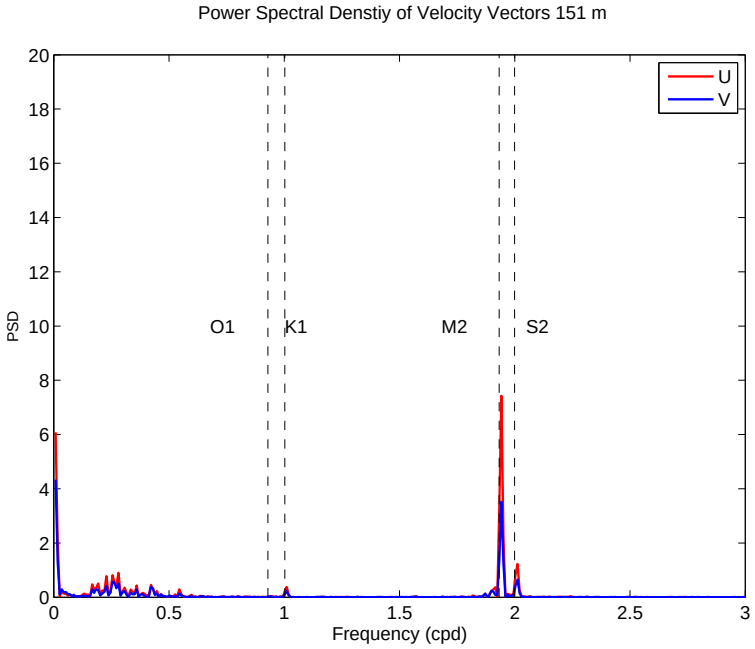

Figure 4.26: Power Spectral Density plot at 151 m, M1.

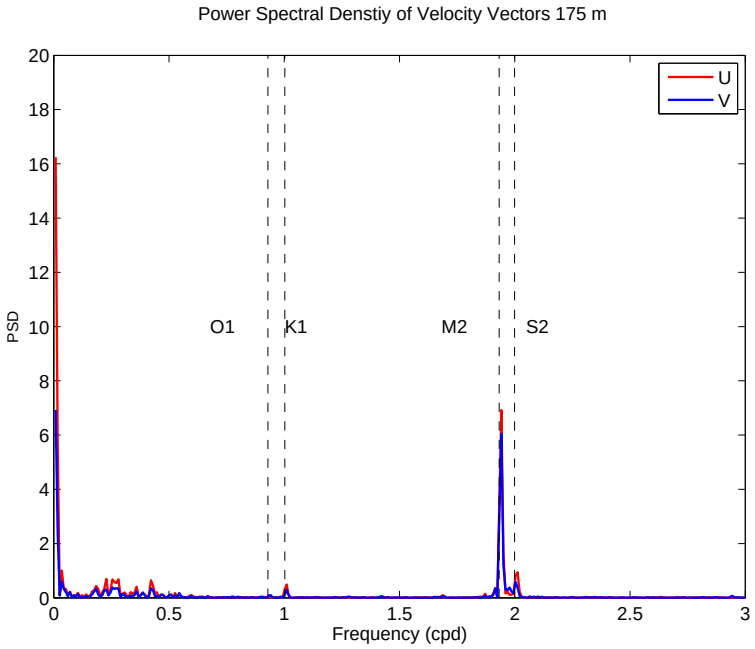

Figure 4.27: Power Spectral Density plot at 175 m, M1.

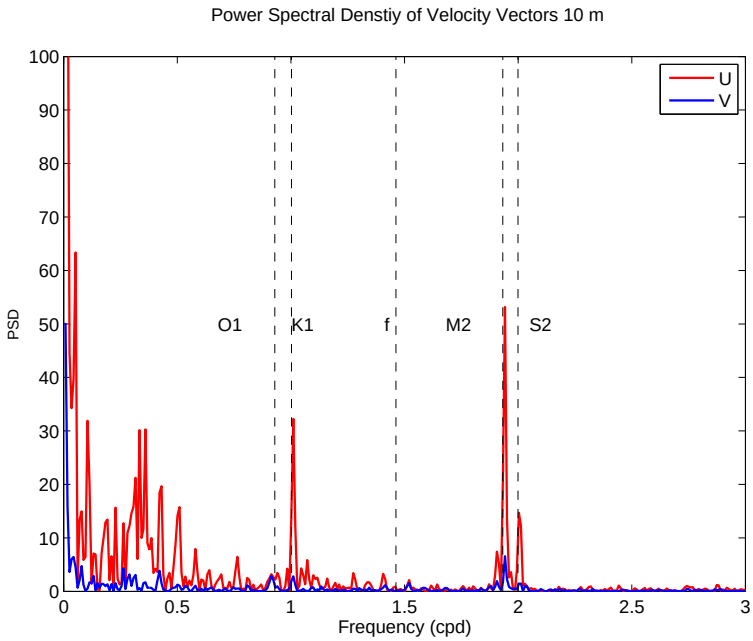

Figure 4.28: Power Spectral Density plot at 10 m, M2.

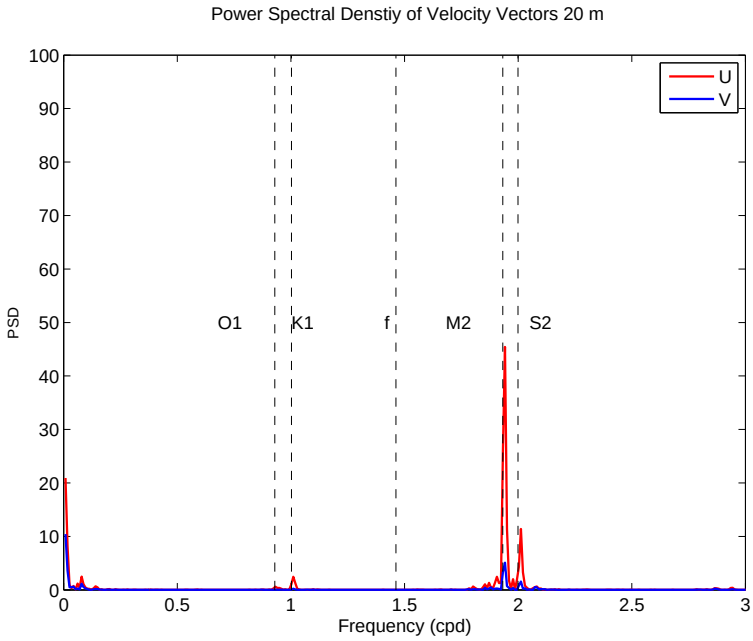

Figure 4.29: Power Spectral Density plot at 20 m, M2.

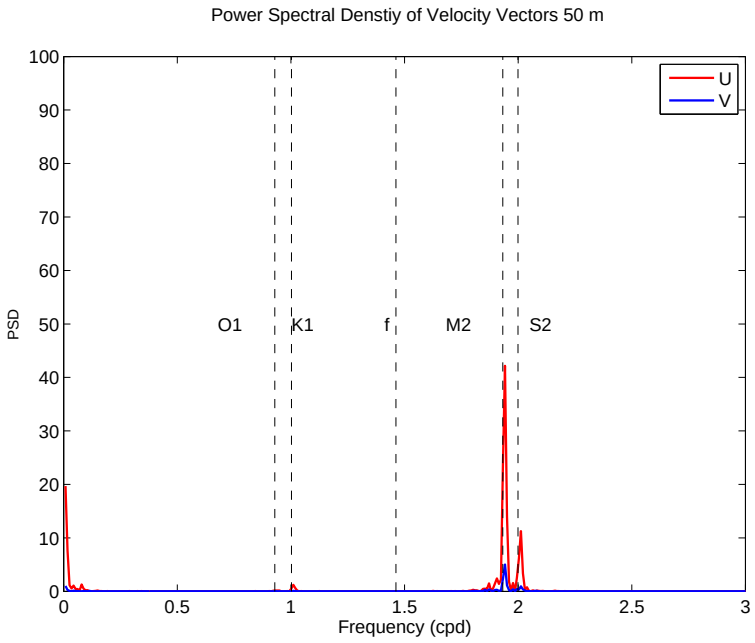

Figure 4.30: Power Spectral Density plot at 50 m, M2.

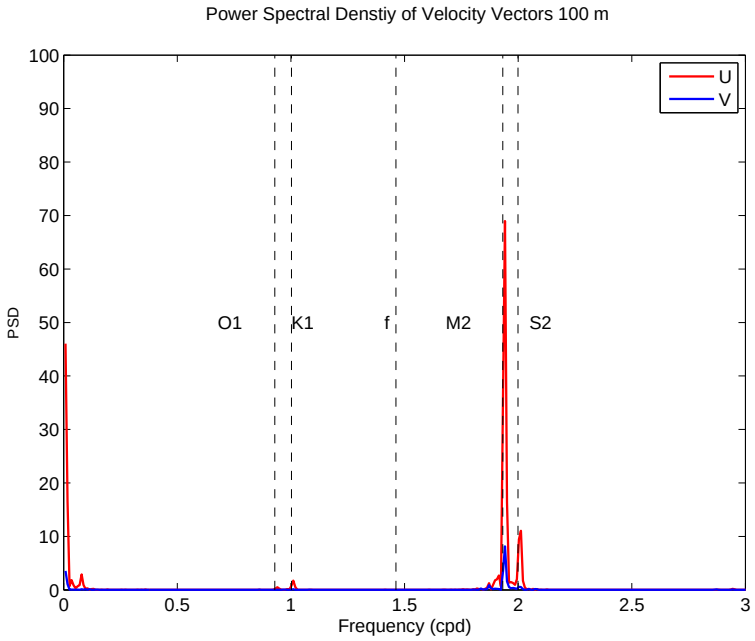

Figure 4.31: Power Spectral Density plot at 100 m, M2.

Table 4.3: M_2 Tidal Constituents at M1 mooring.

Depth (m)	Major Axis (cm/s)	Minor Axis (cm/s)	Inclination (°)	Phase (°)
5	12.416	1.564	37.870	224.510
11	2.348	-0.206	57.550	224.880
15	12.039	-2.189	22.660	224.610
21	2.368	1.050	33.320	226.680
31	5.792	-0.979	7.020	131.410
51	13.809	-1.334	29.630	148.540
75	17.346	-0.580	34.700	180.870
101	15.197	-0.922	38.540	196.990
125	13.098	-0.734	36.520	194.560
151	13.385	-1.388	33.880	192.010
175	14.712	-0.301	42.910	195.110
201	0.209	-0.076	173.370	177.350

Table 4.4: K_1 Tidal Constituents at M1 mooring.

Depth (m)	Major Axis (cm/s)	Minor Axis (cm/s)	Inclination (°)	Phase (°)
5	27.049	9.569	3.970	112.690
11	9.175	2.829	11.840	115.070
15	4.338	-0.168	25.990	16.240
21	3.572	-0.091	43.430	23.160
31	2.523	0.312	30.450	13.370
51	1.019	0.569	177.850	162.110
75	3.086	0.015	36.320	336.180
101	3.251	-0.184	32.800	351.800
125	3.300	0.098	35.690	350.510
151	3.440	0.152	38.010	346.580
175	3.966	0.170	39.310	341.910
201	0.078	0.002	6.790	185.100

Harmonic analysis was performed on the data to separate the tidal constituents and thus gain information on the tidal flow. Two principal lunar semidiurnal M_2 and K_1 are the major constituents at both mooring station. The largest contribution at all depths is from the M_2. Another important result of the harmonic analysis is the rotation angle of the tidal ellipses or hodographs. It gives an estimate of the orientation of the tidal constituents. A negative value for the length of the semi-minor axis indicates that the current rotates clockwise around the tidal ellipse. The values for the M_2 and K_1 constituent at different depths are presented in Tables 4.3, 4.4, 4.5 and 4.6.

The inclinations of tidal ellipses represent the degrees the major axes make with respect to east. The results show that at both Moorings M1 and M2

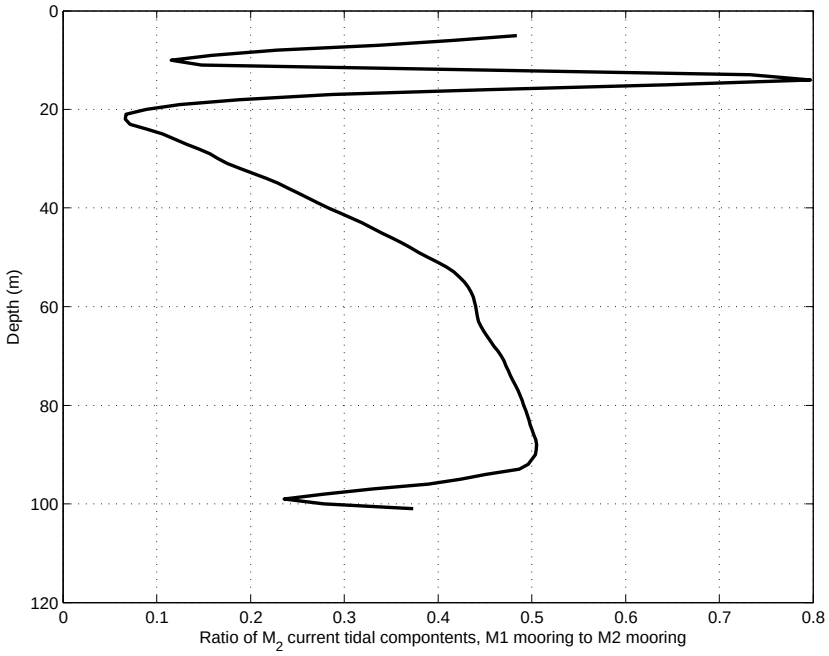

Figure 4.32: Ratio of Tidal harmonics amplitude profiles, M1 to M2.

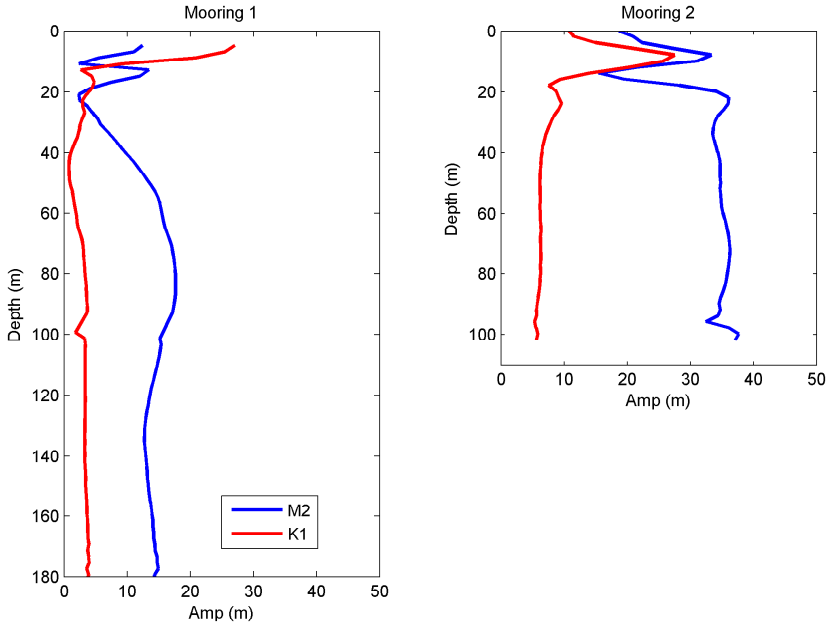

Figure 4.33: Tidal harmonics amplitude profiles at M1 and M2 stations.

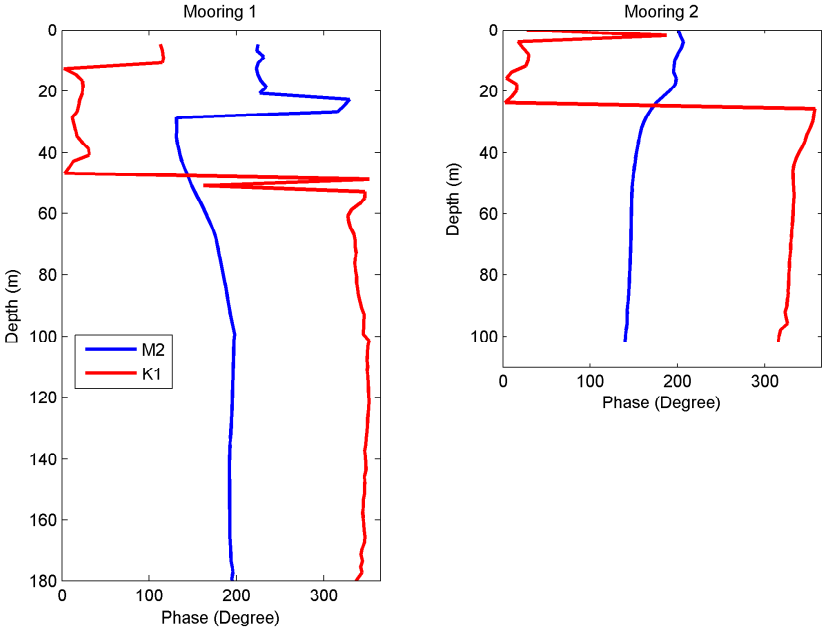

Figure 4.34: Tidal harmonics phase profiles at M1 and M2 stations.

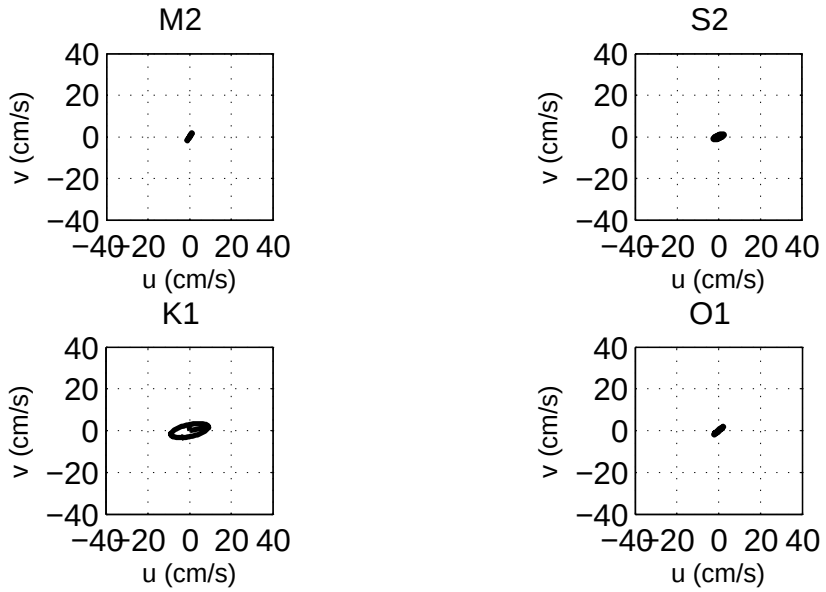

Figure 4.35: Tidal Ellipse of the Current Data at 11 m, M1.

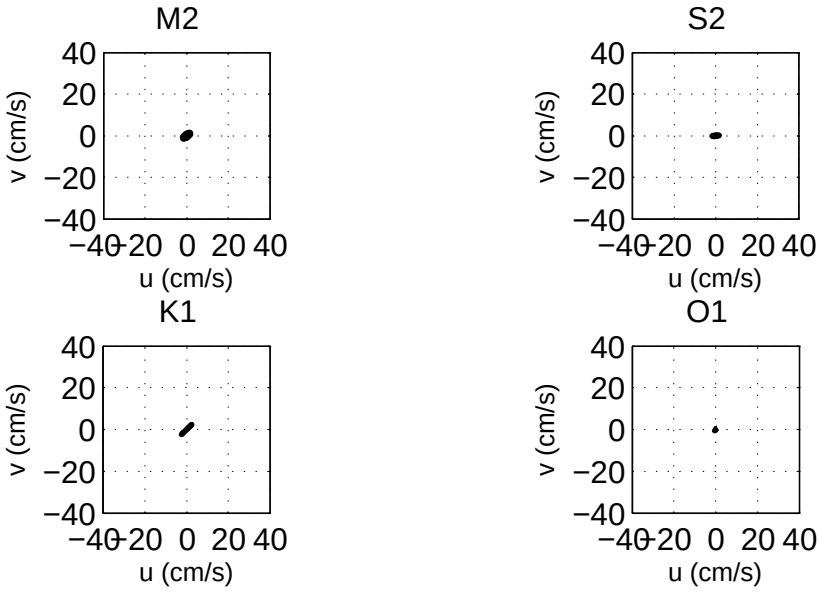

Figure 4.36: Tidal Ellipse of the Current Data at 21 m, M1.

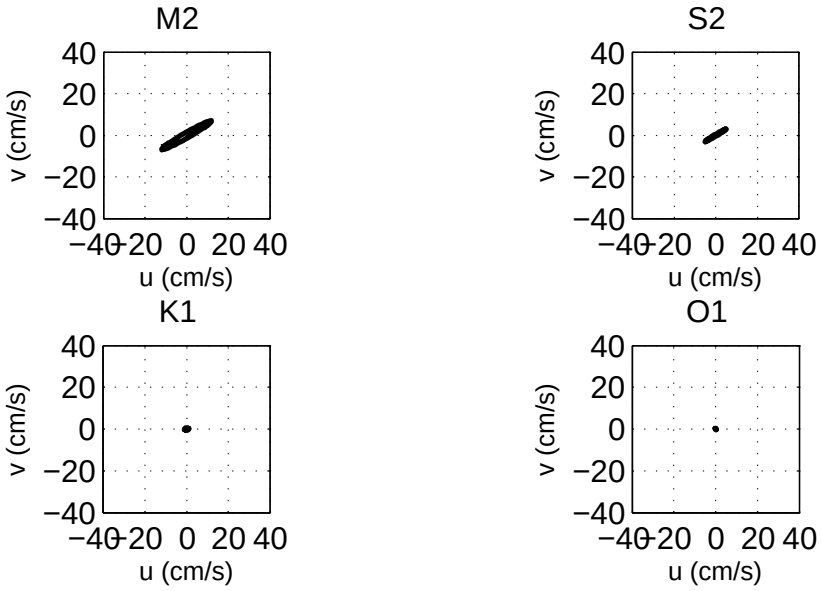

Figure 4.37: Tidal Ellipse of the Current Data at 51 m, M1.

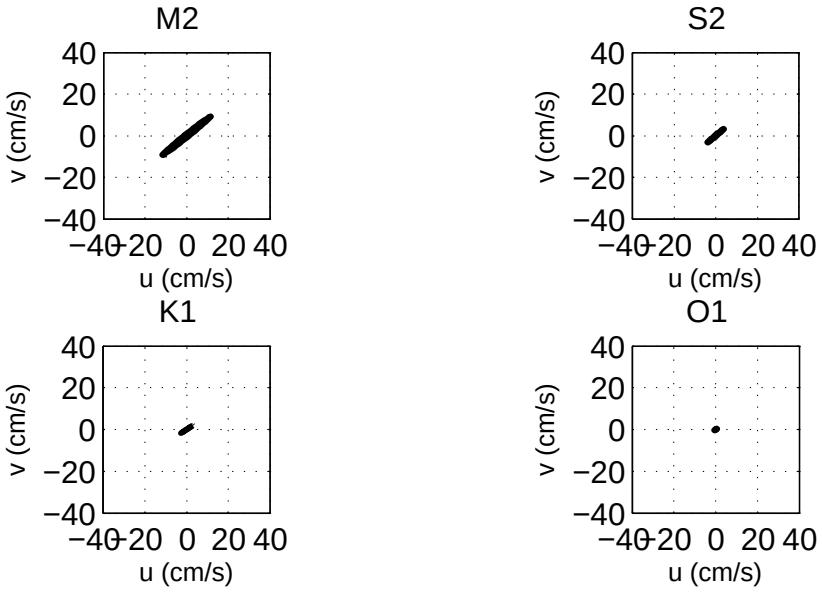

Figure 4.38: Tidal Ellipse of the Current Data at 101 m, M1.

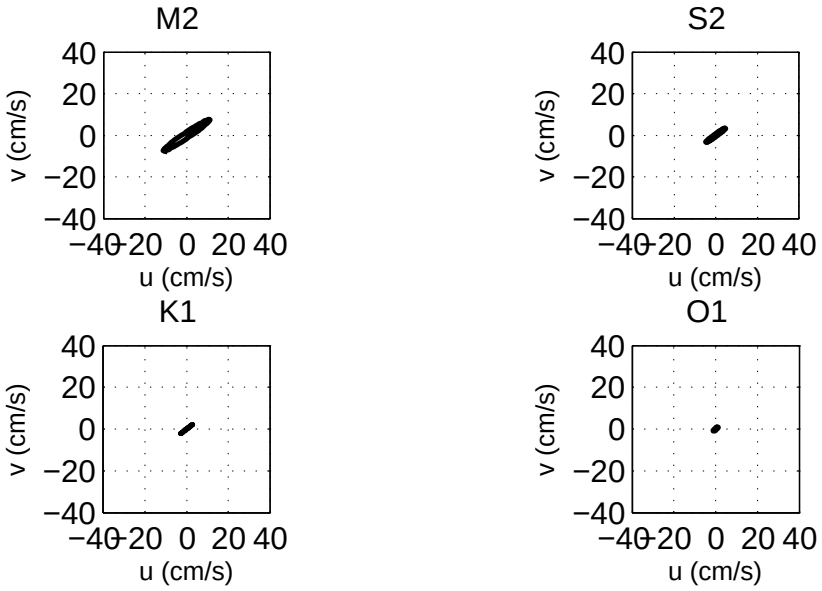

Figure 4.39: Tidal Ellipse of the Current Data at 151 m, M1.

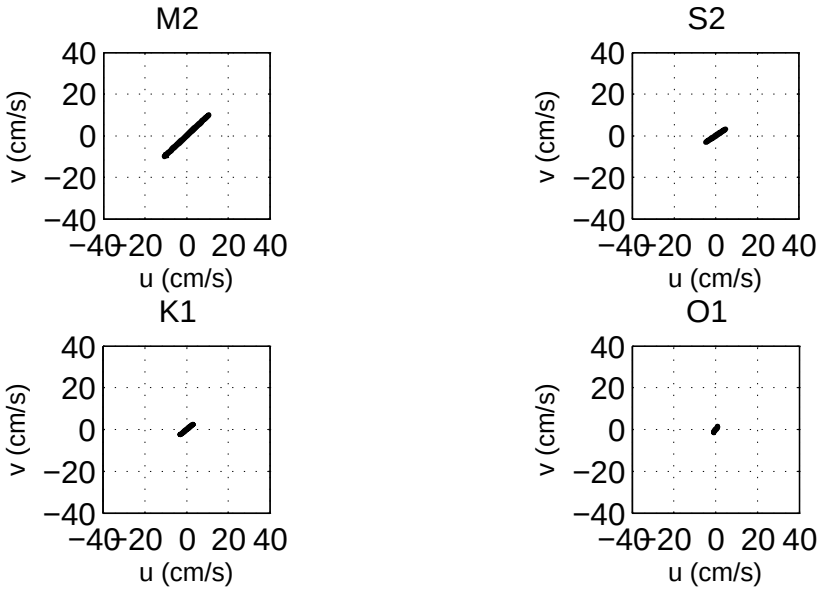

Figure 4.40: Tidal Ellipse of the Current Data at 175 m, M1.

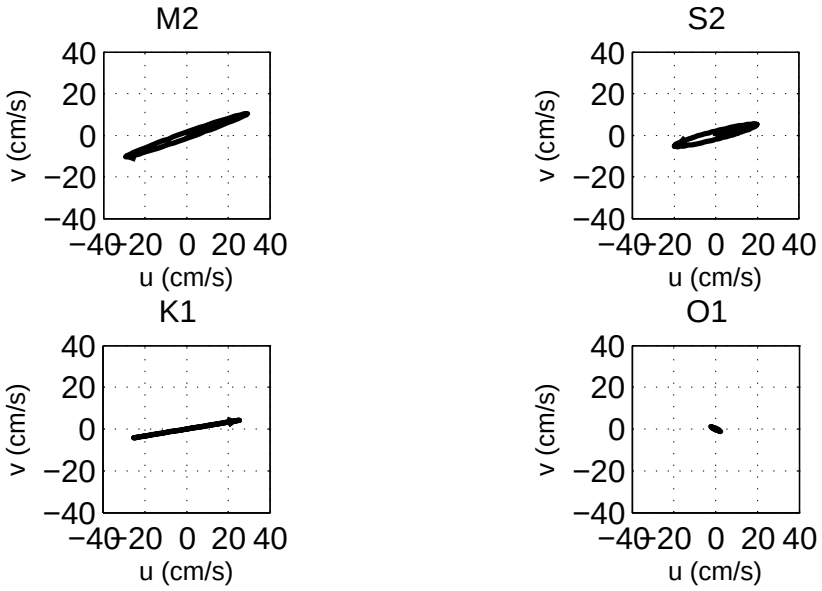

Figure 4.41: Tidal Ellipse of the Current Data at 10 m, M2.

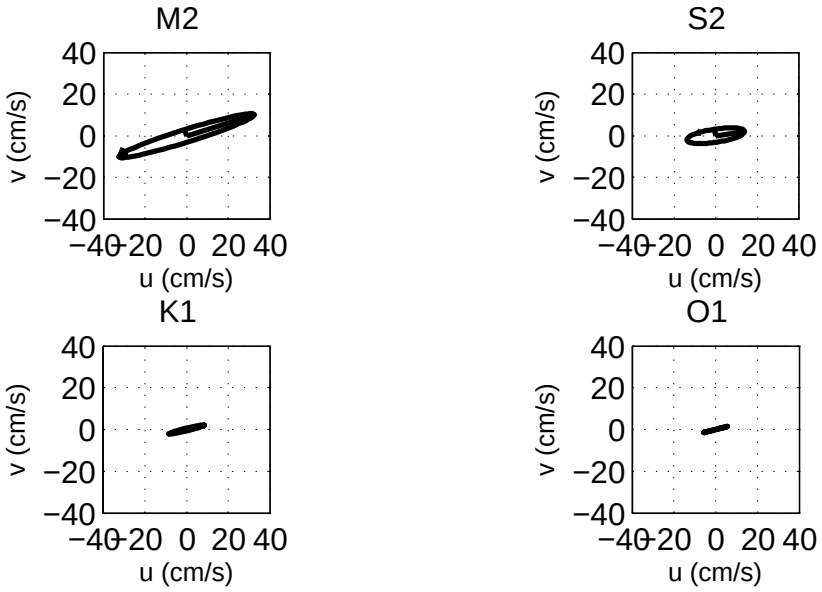

Figure 4.42: Tidal Ellipse of the Current Data at 20 m, M2.

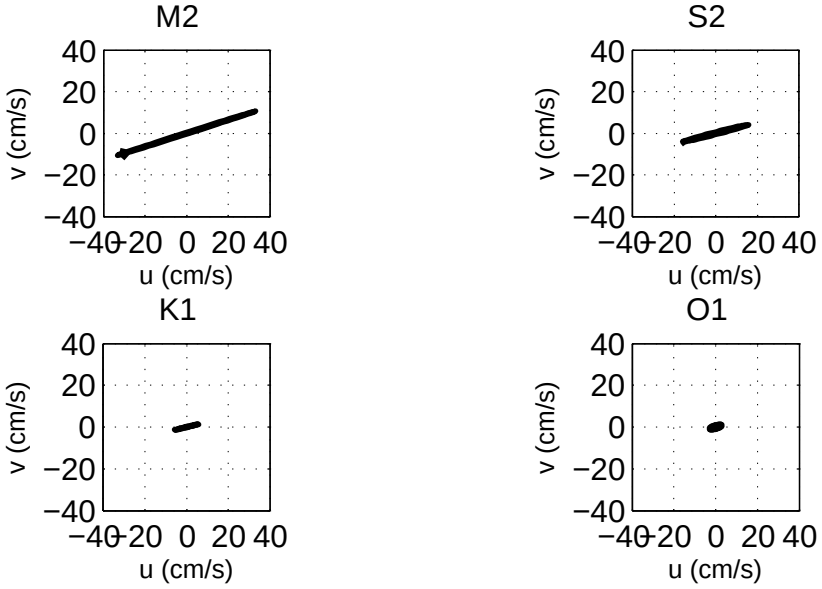

Figure 4.43: Tidal Ellipse of the Current Data at 50 m, M2.

Table 4.5: M_2 Tidal Constituents at M2 mooring.

Depth (m)	Major Axis (cm/s)	Minor Axis (cm/s)	Inclination (°)	Phase (°)
4	22.448	-0.189	17.700	208.820
10	33.219	-0.697	18.360	191.130
14	15.468	2.368	20.230	191.090
20	35.230	2.495	18.260	190.660
30	33.028	-0.112	13.160	162.160
50	33.315	0.515	18.790	149.550
74	35.286	-0.600	14.840	146.540
100	35.823	-1.061	18.430	139.610

Table 4.6: K_1 Tidal Constituents at M2 mooring.

Depth (m)	Major Axis (cm/s)	Minor Axis (cm/s)	Inclination (°)	Phase (°)
4	14.195	-2.261	4.84	24.58
10	26.211	-0.606	16.18	29.27
14	12.684	-0.12	22.46	14.83
20	9.211	0.587	15.43	12.47
30	7.923	-0.595	9.28	355.01
50	6.359	-0.442	14.76	333.69
74	6.695	-1.134	8.55	326.27
100	5.73	-0.905	12.24	313.75

the tidal currents were aligned along the axis of Narrows/Channels throughout the water column. The small amplitudes of the minor axes indicate a weak cross-channel flow.

At Location M1, magnitude of M_2 was suppressed by outward surface flow near the surface and reduced to about 2.3 cm/s at 20 m depth. Below 20 m magnitude of M_2 increased with depth and reached its maximum of 17 cm/s at about 80 m depth. Almost all M_2 tidal energy was dissipated traveling through the narrows near the top 20 m. The remained M_2 tidal energy was then reflected to the deeper layer of the water column (Figures 4.33 and 4.34).

At Location M2, the magnitude of M_2 was about 30 cm/s throughout the water column.

For both locations, magnitude of K_1 near the surface was about 28 cm/s and indicate that the K_1 tidal wave passed the Narrows without significant energy absorption (Figures 4.33 and 4.34).

Figure 4.32 shows ratio profile of M_2 tidal current components (major axes of tidal ellipses) at two moorings. About 80 percents of tidal energy can pass the Narrow between depth 12 m to 15 m, where the tidal amplitude reaches a minimum of 15 cm/s at M2 mooring (Figure 4.33). At other depths, the ratio of tidal energy passed the Narrows was between 20 to 50 percents.

Tidal ellipses for different depths at both locations are presented in Figures 4.35 - 4.44.

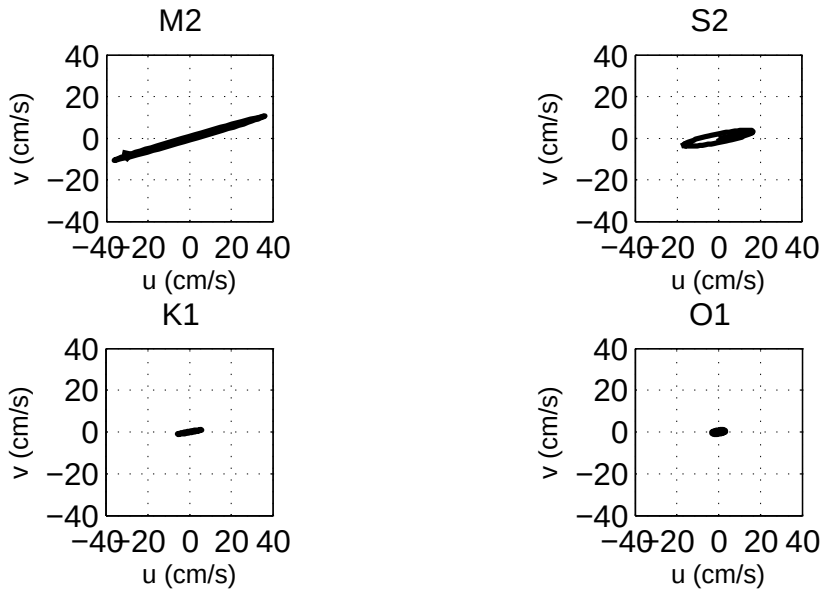

Figure 4.44: Tidal Ellipse of the Current Data at 100 m, M2.

4.6 Temperature recorded of thermistors

Figures 4.45 and 4.46 show depth-time contour plots of temperature derived from thermistors instruments. A low pass Butterworth filter was applied to raw records with cutoff period of 24 hours.

At location M1, surface layer was dominated by warm water of above 15°C with a dominant frequency of about 3 to 4 days. Temperatures steadily decreased with depth to 0°C at a depth of 120 m. The temperature then stay at 0°C thereafter with deeper water. Vertical motions of isotherm indicates energetic internal wave propagation.

At location M2, warming surface layer can also be found. Surface Temperature increased from about 1°C at the beginning of mooring to about 5°C around day 230. An upwelling event happened around day 240 and temperature dropped to 2°C.

4.7 CTD Cast profiles

Figures 4.47, 4.48 and 4.49 shows the temperature, salinity and density profile of CTD transect taken along the center of the lake (Figure 2.1). The stratification in the lake was well defined as those profiles showed a fresh, warm surface layer of about 20 m thick inside the lake. The fresh surface layer became thinner toward the Narrows and almost disappeared outside the Narrows. a strong

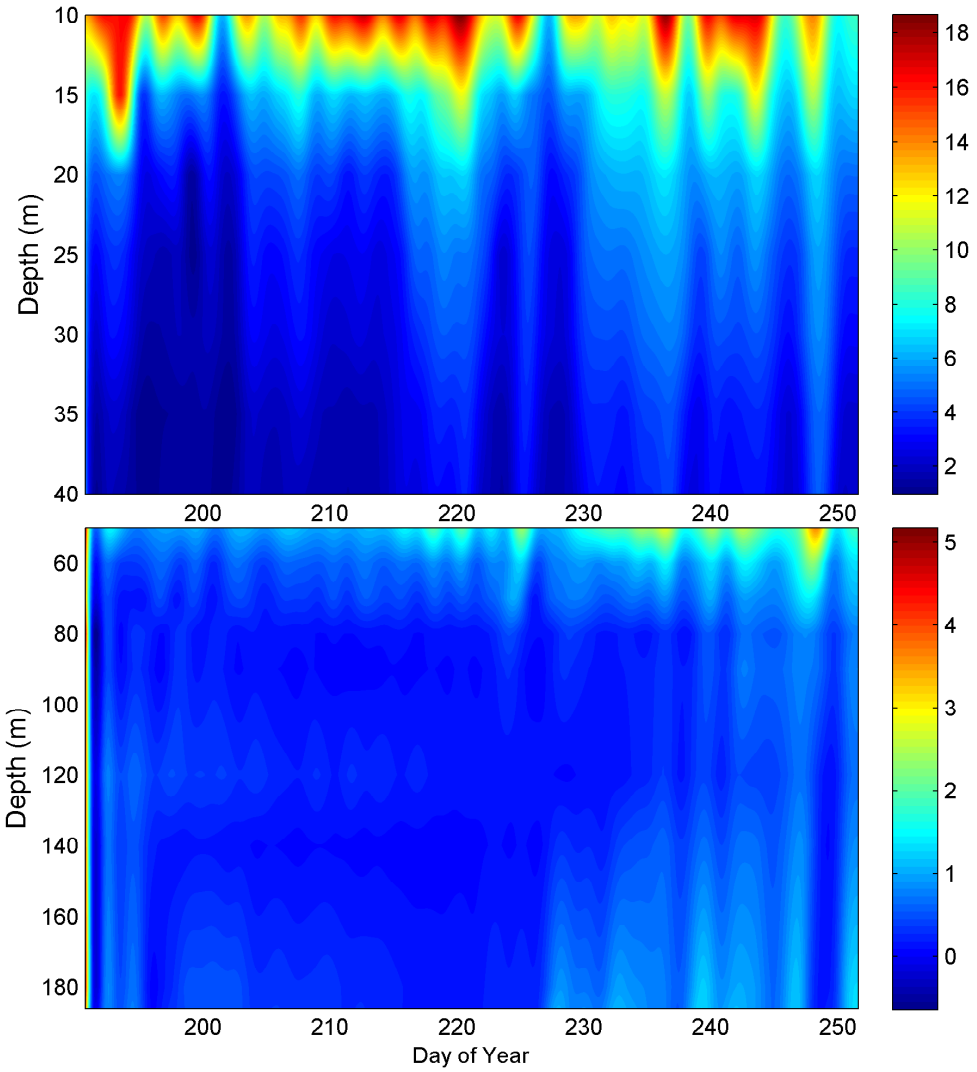

Figure 4.45: Contour plot of temperature at M1, unit in ° C.

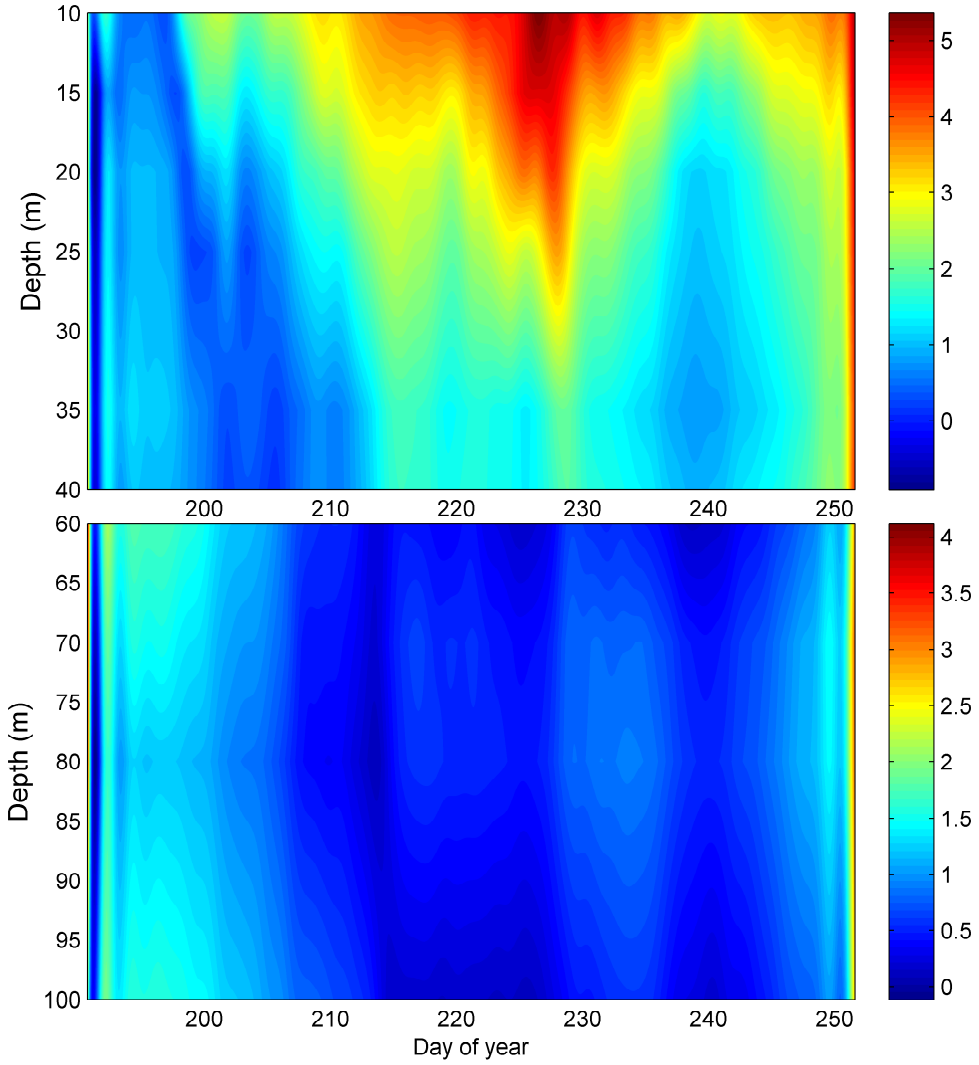

Figure 4.46: Contour plot of temperature at M2, unit in ° C.

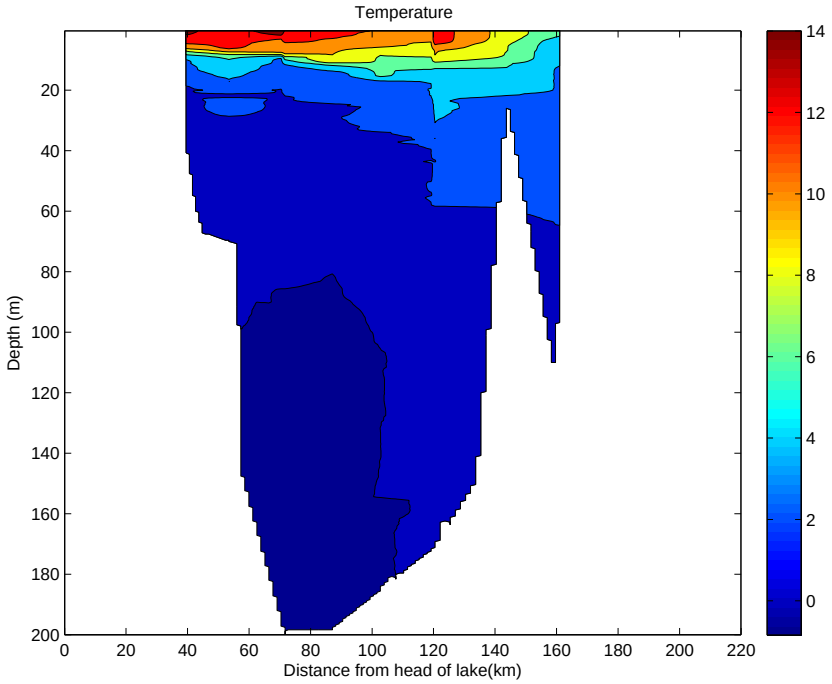

Figure 4.47: Temperature profiles taken along the center of the lake and Narrows, unit in $^{\circ}C$.

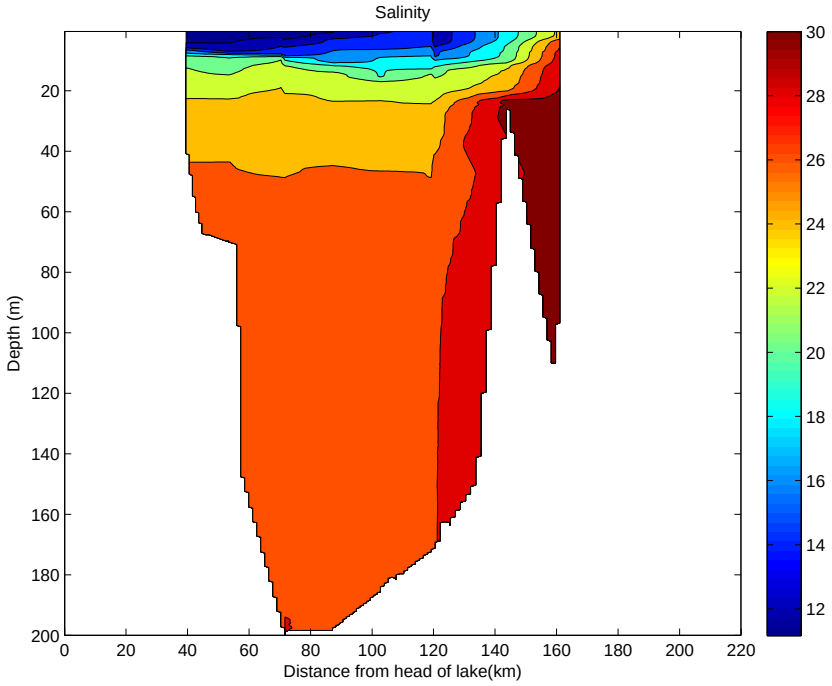

Figure 4.48: Salinity profiles taken along the center of the lake and Narrows, unit in PSU.

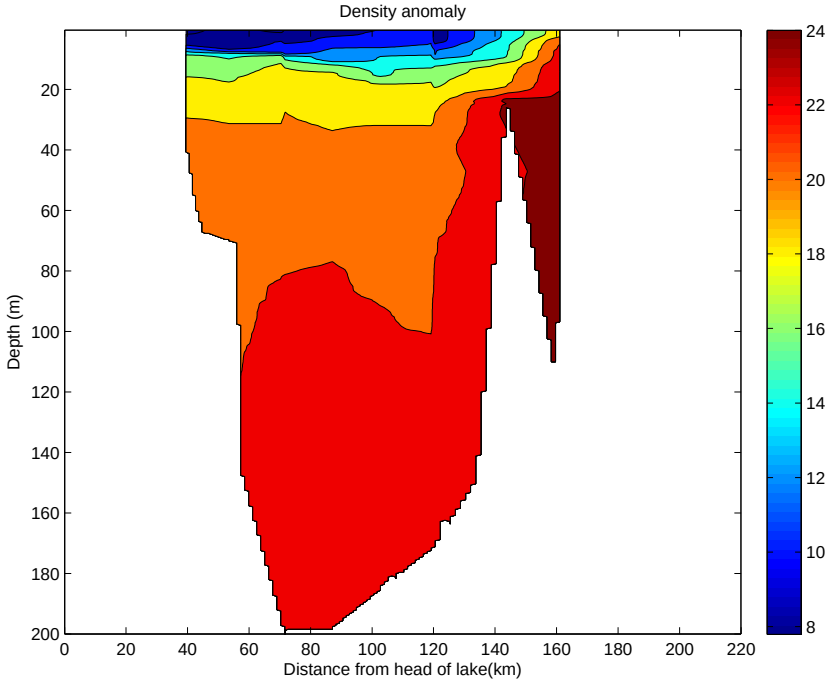

Figure 4.49: Density anomaly profiles taken along the center of the lake and Narrows, unit in kg/m^3.

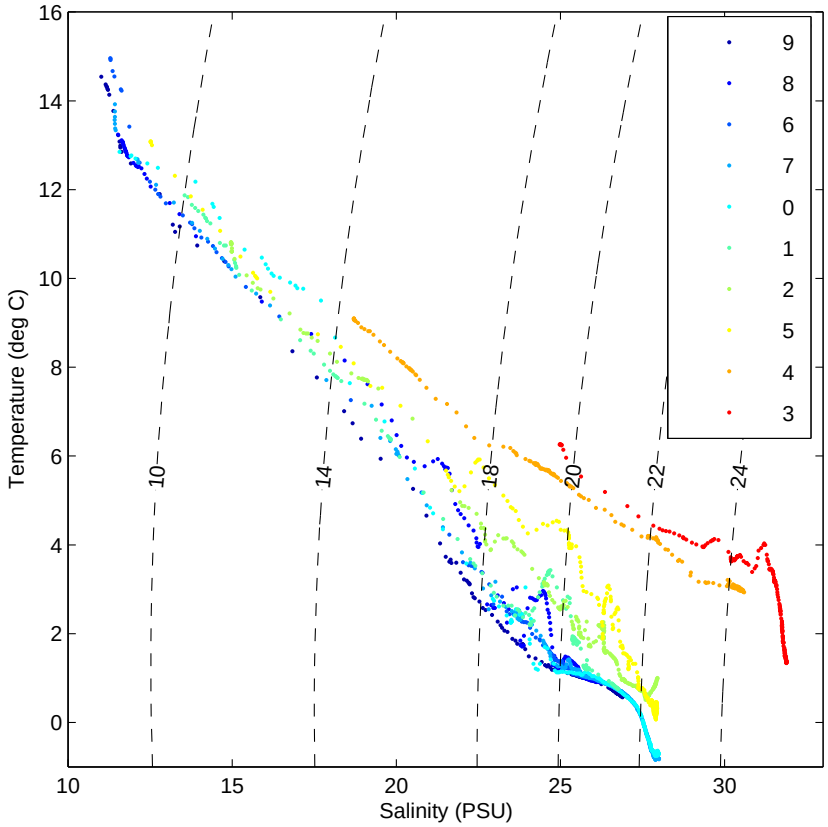

Figure 4.50: T-S diagrams of CTD data collected along the center of the lake and Narrows. (Red:Cast 3 outside the Narrows; Green: Cast 4 over the sill in the middle of Narrows.)

density gradient had developed below the fresh surface layer.

The T-S diagrams in Figure 4.50 show two distinct water masses and strong stratification. Water properties exchanged between surface fresh and bottom saline water mass, with mixing across density surfaces for most of those locations except Cast 3 (outside of the lake). At Cast 3, bottom water mixing happened along density surface and indicating an intrusion and mixing by the Labrador Sea water.

4.8 Atmospheric records at Happy Valley-Goose Bay

Figures 4.51, 4.52 and 4.53 show atmospheric records at the nearby Happy Valley-Goose Bay weather station. Wind roses from the Happy Valley-Goose

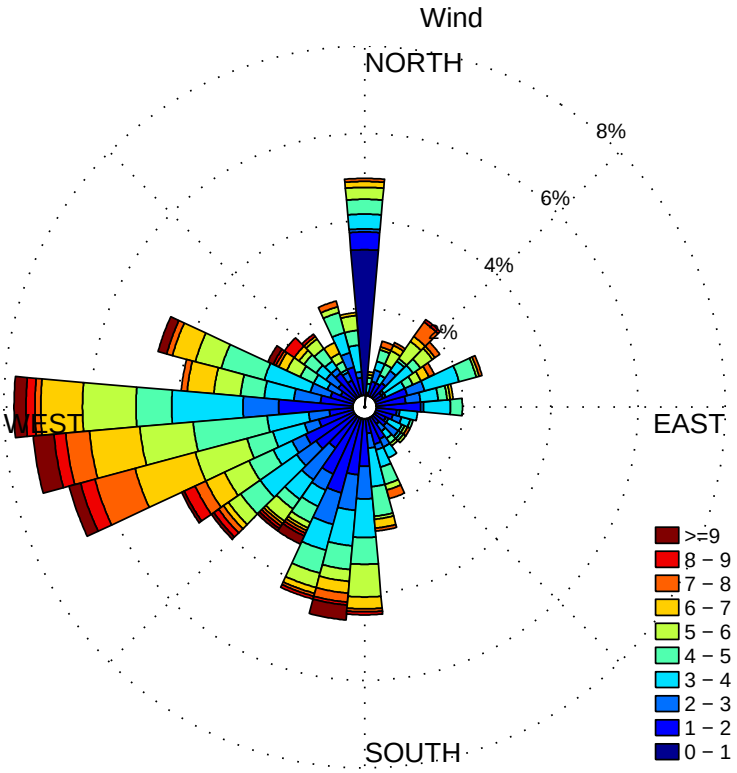

Figure 4.51: Current rose of wind at Goose bay, Labrador, unit in m/s.

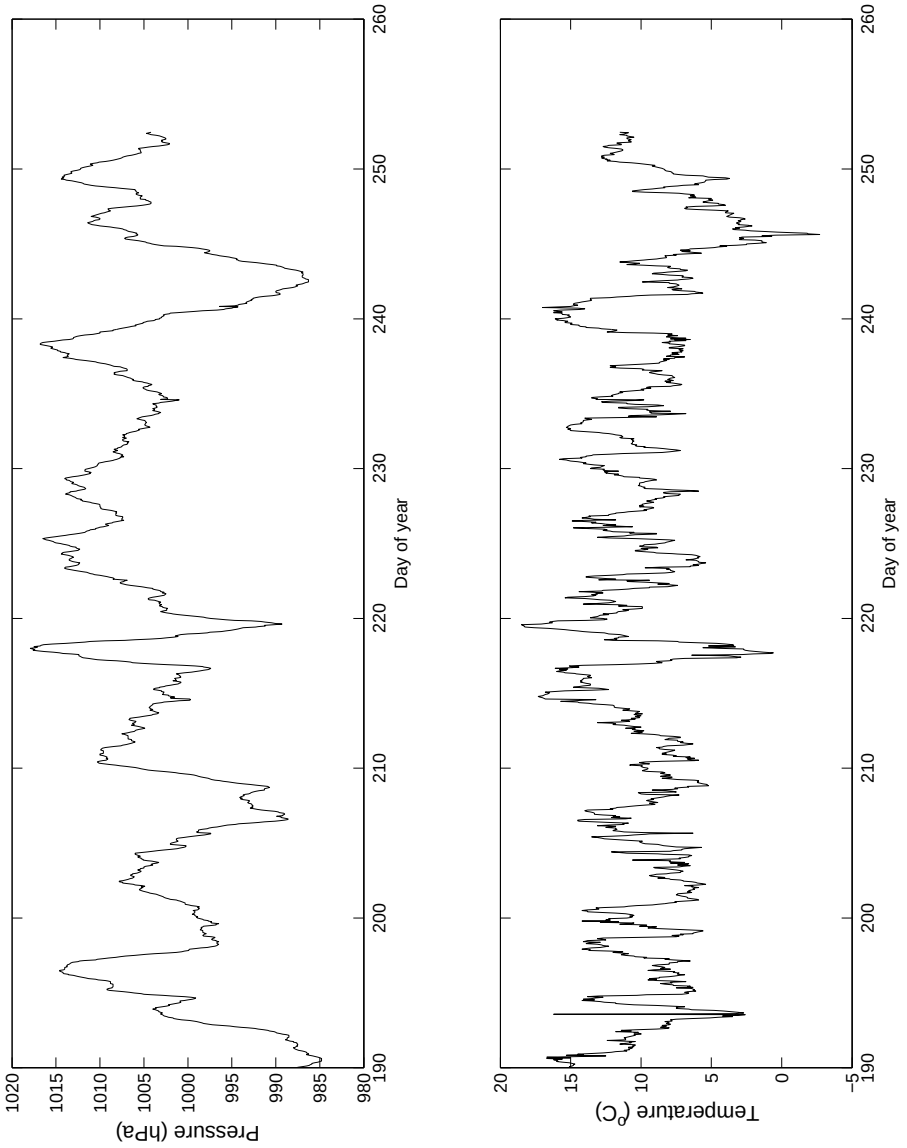

Figure 4.52: Air pressure and temperature at Goose bay, Labrador.

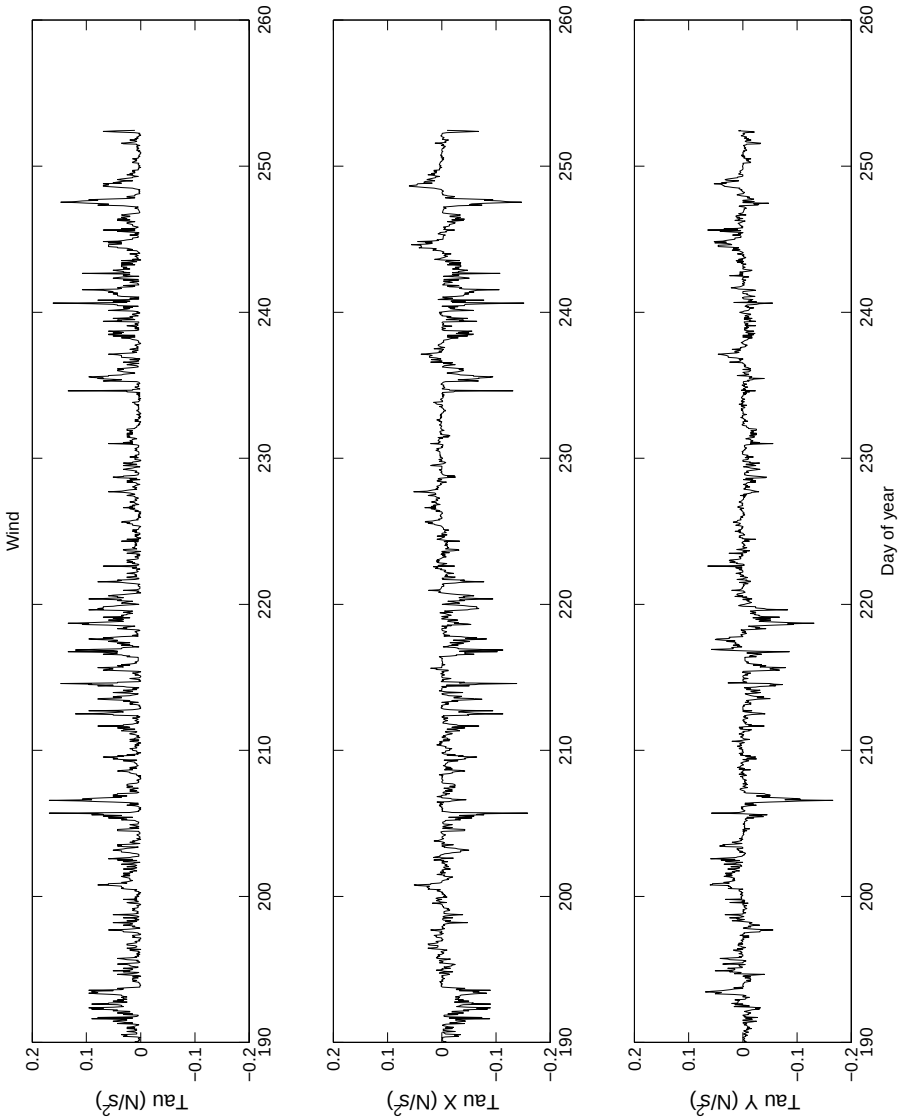

Figure 4.53: Wind stress at Goose bay, Labrador.

Bay weather station are shown in Figure 4.51. These preferred wind direction are west and southwest for the mooring period.